Pyrite nanoparticles derived from mine waste as efficient catalyst for the activation of persulfates for degradation of tetracycline

Rahimi, Farzaneh; van der Hoek, Jan Peter; Royer, Sebastien; Javid, Allahbakhsh; Mashayekh-Salehi, Ali; Jafari Sani, Moslem

DOI
10.1016/j.jwpe.2020.101808

Publication date
2021

Document Version
Final published version

Published in
Journal of Water Process Engineering

Citation (APA)
Rahimi, F., van der Hoek, J. P., Royer, S., Javid, A., Mashayekh-Salehi, A., & Jafari Sani, M. (2021). Pyrite nanoparticles derived from mine waste as efficient catalyst for the activation of persulfates for degradation of tetracycline. *Journal of Water Process Engineering*, *40*, 1-16. Article 101808. https://doi.org/10.1016/j.jwpe.2020.101808

Journal of Water Process Engineering 40 (2021) 101808

Contents lists available at ScienceDirect

Journal of Water Process Engineering

journal homepage: www.elsevier.com/locate/jwpe

Pyrite nanoparticles derived from mine waste as efficient catalyst for the activation of persulfates for degradation of tetracycline

Farzaneh Rahimi [a], Jan Peter van der Hoek [b], Sebastien Royer [c], Allahbakhsh Javid [d], Ali Mashayekh-Salehi [d,*], Moslem Jafari Sani [e]

[a] Student Research Committee, School of Public Health, Shahroud University of Medical Sciences, Shahroud, Iran
[b] Department of Water Management, Delft University of Technology, Delft, the Netherlands
[c] Univ. Lille, CNRS, Centrale Lille, Univ. Artois, UMR 8181, UCCS, Unité de Catalyse et Chimie du Solide, F-59000, Lille, France
[d] School of Public Health, Shahroud University of Medical Sciences, Shahroud, Iran
[e] School of Medicine, Shahroud University of Medical Sciences, Shahroud, Iran

ARTICLE INFO

Keywords:
In-vivo toxicity
Peroxymonosulfate
Emerging contaminants
Sulfate radicals
Tetracycline

ABSTRACT

Pyrite mine waste was used as a non-toxic and natural catalyst for the activation of peroxydisulfate (PDS) and peroxymonosulfate (PMS) to oxidize tetracycline (TTC), one of the most extensively used antibiotics worldwide, in contaminated water. The results demonstrated that PMS was activated more effectively than PDS by using pyrite. Scavenging experiments indicated that both $OH^{\bullet}$ and $SO_4^{\bullet-}$ were the main oxidative species in the pyrite/PMS process, while $SO_4^{\bullet-}$ was more dominant. A high degradation of 98.3 % and significant mineralization (up to 46 %) of TTC (50 mg/L) were achieved using pyrite activated PMS at a reaction time of 30 and 60 min, respectively. In-vivo toxicity of raw and pyrite/PMS treated TTC solutions was evaluated using biochemical and histopathological assays. The results revealed that the pyrite/PMS process significantly decreased the nephrotoxicity (90 %) and hepatotoxicity (85 %) effect of TTC. Catalyst reusability was evaluated under cycling conditions. No significant decrease in process efficiency was measured between the first and fourth cycle (<3% decrease in TTC removal). In conclusion, mine waste pyrite nanoparticles can be considered as a non-toxic and clean catalyst to activate PMS for an effective detoxification, degradation, and intermediate mineralization of TTC, as a refractory water pollutant.

1. Introduction

In recent decades, the presence of organic recalcitrant matter such as pharmaceutical compounds (PCs) as emerging contaminants in water has attracted increasing attention [1–4]. The prevalence of these refractory contaminants has unexpected and sublethal chronic effects on human beings and ecosystems [5–7]. In recent years, advanced oxidation processes (AOPs) based on sulfate radicals ($SO_4^{\bullet-}$) have gained attention for the degradation of recalcitrant pollutants [8–10]. Several advantages have been reported for these technologies including long lifetime, high oxidation potential ($E_0 = 2.5–3.1$ V) and relative stability of $SO_4^{\bullet-}$ [11,12]. $SO_4^{\bullet-}$ is produced mostly through the activation of persulfates (PS) (peroxydisulfate (PDS) and/or peroxymonosulfate (PMS)), via UV radiation [13], heat [14], carbon catalyst, ultrasound, electrochemistry, and transition metals (such as Fe^{2+}, Co^{2+}, Ag^{+}, and Cu^{2+}) [15–18]. Recent studies have proven that PS activation by transition metals could generate both $SO_4^{\bullet-}$ and $OH^{\bullet}$ simultaneously [12,19]. This process leads to high efficiency in the decomposition of various water pollutants. Among various transition metals used for activating PS for the production of $OH^{\bullet}$ and $SO_4^{\bullet-}$, Fe-containing compounds such as Fe_2O_3-Cu_2O [15], $MnFe_2O_4$ [20], $CoFe_2O_4$ [21,22], and FeS_2 [23,24] have attracted attention. These compounds have special properties including high efficiency, natural abundance and nontoxicity.

PS-based AOPs with ionic Fe as a catalyst are classified into homogenous and heterogeneous systems. Some recurrent limitations exist for homogeneous systems including difficult recovery of Fe ions, important effect of pH on the performance, slow recovery of Fe(II)/Fe(III) and rapid scavenging of $SO_4^{\bullet-}$ by Fe^{2+} excess [25,26]. Thus, recently, heterogeneous PS-based AOPs with Fe have been considered in the treatment of water refractory contaminants [27–29]. In this regard, most of the previous studies have employed synthetic iron composites. Although some of these synthesized catalysts have demonstrated

* Corresponding author.
E-mail address: mashayekh@shmu.ac.ir (A. Mashayekh-Salehi).

https://doi.org/10.1016/j.jwpe.2020.101808
Received 18 October 2020; Received in revised form 12 November 2020; Accepted 16 November 2020
Available online 30 November 2020

considerable potential for PS activation, their production may be problematic from an environmental point of view leading to a limited application in full-scale systems [30]. To overcome these limitations, the use of natural Fe-containing minerals could be considered as a feasible option.

Among different Fe natural minerals, pyrite (FeS_2) is considered as one of the most abundant natural iron-sulfur minerals available from natural ore as a mine waste [22,31,32]. Therefore, due to the low-cost and environmental friendly characteristics, waste-derived pyrite can be considered as a catalyst for water and wastewater treatment. Many researchers have confirmed the cost-effectiveness of pyrite as a catalyst for the removal of water pollutants [33,34]. Moreover, pyrite is stable and has a low solubility in water. The stability and reusability of pyrite have been proven in the heterogeneous Fenton-like pyrite/H_2O_2 process [22]. Because of unique features of pyrite, it may be an attractive Fe containing natural material for the activation of PDS and PMS and, thus, for the production of an enhanced amount of $OH^{\bullet}$ and $SO_4^{\bullet -}$. Although numerous studies have demonstrated that pyrite could be effectively used as a heterogeneous catalyst for the efficient removal of organic compounds from water [22,24,35–38], to the extent of our knowledge no information is available on the use of pyrite mine waste as catalyst for the removal of pharmaceutical compounds as water emerging contaminants. Moreover, no study has compared the pyrite/PDS and pyrite/PMS systems for tetracycline (TTC) degradation.

TTC ($C_{22}H_{24}N_2O_8$) is one of the most extensively used antibiotics [39,40]. This antibiotic is frequently detected in surface water resources which receive run-off from wastewater treatment plants and agricultural lands [41–44]. TTC can inhibit bacterial protein synthesis and contributes to the spread of resistant genes and bacteria [45,46]. Moreover, TTC has toxic effects on kidney and liver cells [47]. Thus, the presence of TTC in the environment has adverse effects on microbial community and human health [49]. Although several studies have reported recently the successful removal of TTC [50–52], clearly further research is needed in this area. Several studies have investigated persulfate activation by pyrite for degradation of organic pollutants. However, no study has been conducted on TTC degradation by pyrite/persulfate so far. In addition, in-vivo toxicity has never been considered for degraded pollutants via sulfate-radicals based processes. This study is the first attempt for demonstrating the performance of PS/pyrite in TTC degradation in terms of the efficiency, kinetics and toxicity evaluation.

Accordingly, the hypothesis of the present study is that pyrite derived from mine waste is an effective and clean, non-toxic catalyst to activate PS for the degradation of TTC as a model of recalcitrant water contaminants. The main goals of this study were: (1) determining the catalytic potential of waste pyrite in activating PDS and PMS for the generation of reactive species; (2) evaluating various operational conditions (pH, pyrite dosage, persulfate dosage, initial TTC concentration, temperature and presence of solubilized ionic species); (3) assessing the contribution of free radicals in degradation reactions; (4) determining the degradation and mineralization kinetics of TTC in the pyrite/PMS process; (5) examining the nephrotoxicity and hepatotoxicity effects of raw and pyrite/PMS -treated TTC solutions in-vivo under optimum operational parameters.

2. Materials and methods

2.1. Materials

Pure tetracycling (TTC) powder was purchased from a local pharmaceutical company (Daro Pakhsh, Iran). To prepare a stock TTC solution, 1 g of pure TTC powder was dissolved in 1 L of deionized water (0.1 %) and stored for future applications at 4℃. The working solutions were prepared by diluting the aliquots of the TTC stock solution using deionized water to obtain the desired concentration. All the chemicals in this study were of analytical grade. PDS ($Na_2S_2O_8$) and PMS ($2KHSO_5.KHSO_4.K_2SO_4$) were obtained from Merck and Sigma-Aldrich, respectively, and were used according to the instructions. The PDS and PMS concentrations used in the experiments were calculated based on $S_2O_8^{2-}$ and $(H_3O_{18}S_4)^{5-}$ concentrations, respectively.

2.2. Catalyst preparation and characterization

The natural pyrite nanoparticles were prepared from local mine waste. The pyrite was grounded using an agate mortar instrument and afterward sieved to gain microparticles smaller than 50 μm. Ultrasonication (20 kHz) was used to remove impurities and then the material was washed with 0.5 M nitric acid to eliminate oxidized surface. To prepare nano size pyrite particles, the microparticles were additionally grounded by a ceramic mortar at a rotation speed of 300 rpm for 1 h. Then it was milled with the Planetary Ball Mill (PBM-230 Nanosatco model). The nano size particles were rinsed with ethanol and deionized water (50/50) for 3 times to remove any remaining impurities and then dried in a furnace at 105 °C for 3 h.

The prepared nanoparticles were characterized for surface morphology, chemical composition, crystalline shape, surface functional groups, structural composition and distribution of nanoparticles. Details of experimental techniques utilized for characterization of the nanopyrite catalyst are presented in SI (Supplemental Information).

2.3. Experimental procedures

The TTC removal experiments were conducted using bench-scale reactors, 100 mL Pyrex Erlenmeyer flasks, schematically shown in Fig. 1 at an ambient temperature (25 ± 2 ℃). To investigate the catalytic activity of pyrite nanoparticles, the TTC removal was measured for adsorption onto pyrite, for sole PDS, sole PMS, pyrite/PDS, and pyrite/PMS, separately, and calculated according to Eq. (1):

pyrite activity (%) = TTC degradation in pyrite/PS - (TTC degradation by sole PDS/PMS + TTC adsorption onto pyrite) (1)

For all tests, a 50 mL volume of working solution with desired initial TTC concentration and solution pH was introduced to the reactor and, then, each agent with desired dosage (pyrite, PDS, PMS) was added. Afterwards, the reactor content was stirred magnetically at 100 rpm to prepare appropriate-mixed suspension for a specific time period. The solution pH was adjusted by using Normal HCl and NaOH buffers. At end of each reaction, the oxidation reaction was quenched by adding 1 mL of sodium thiosulfate (1 M) to the sample [1,53]. Since phosphate and carbonate species could quench the reactive radicals, no buffer species were added to the reaction solution (except for inorganic ions

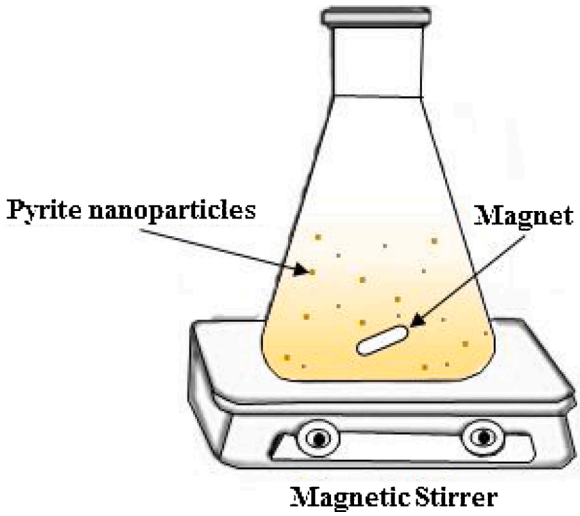

Fig. 1. The schematic of experimental setup.

experiments). Finally, the quenched mixture was filtered through a 0.22 μm MCE membrane (Jet Biofil), and then used for the analysis of the target parameters. Effect of several experimental conditions on TTC degradation were investigated, including the type of PS (PSD and PMS), solution pH (3−10), pyrite and PMS dosage (0.2−2 g/L), TTC initial concentration (25−500 mg/L), solution temperature (15, 25, 40 ℃), and ions in the water phase. In addition, the degradation and mineralization rates of TTC by pyrite/PMS process as well as associated reaction kinetics were compared with those in the sole PMS process. Moreover, the reusability potential of the catalyst in the pyrite/PMS process was examined.

All experiments were carried out in duplicate and the results are presented as the mean ± standard deviation of two independent experiments.

2.4. Analysis of target compounds

The TTC concentrations, before and after the reaction, were measured using a high-performance liquid chromatography device (HPLC, Agilent Co.) equipped with a UV detector. The wavelength for TTC detection was 385 nm. The separation was performed using a C18 column (Eclipse plus C18 column; 3.5 μm, 4.6 × 100). A combination of 40 % acetonitrile and 60 % phosphate buffer (v/v), at pH 4.8, was used as mobile phase. The flow rate of mobile phase injection was adjusted to 0.5 mL/min.

The TTC degradation percentage was evaluated using Eq. (2):

$$\text{TTC degradation } (\%) = \frac{(TTC_0 - TTC_t)}{TTC_0} \times 100 \quad (2)$$

Where TTC_0 and TTC_t show the TTC concentration at time 0 (initial) and at reaction time t (final), respectively. The initial total organic carbon (TOC_0) concentration and the final total organic carbon (TOC_t) concentration in the samples treated by sole PMS and pyrite/PMS processes under optimum operational conditions, was determined with the use of a TOC analyzer (Shimadzu Co, VCSH Model). A 25 mL sample was taken for each TOC analysis. The measurements were done in duplicate for each sample and average values were reported. The TTC mineralization percentage was determined by the TOC reduction, calculated using Eq. (3):

$$\text{TTC mineralization } (\%) = \frac{(TOC_0 - TOC_t)}{TOC_0} \times 100 \quad (3)$$

The concentrations of Fe^{2+} and total iron (Fe^{2+} and Fe^{3+}) leached from the pyrite into the reaction solution were respectively measured using the 1,10-phenanthroline method and atomic absorption spectroscopy (AAS) based on the Standard Methods [54].

2.5. In-vivo toxicity

Toxicity is generally classified into chronic toxicity and acute toxicity. Present study was focused on the acute type. For this, the in-vivo toxicity (hepatotoxicity and nephrotoxicity) assessments of raw and pyrite/PMS treated (under optimum condition) TTC solutions were carried out in terms of biochemical and histopathological assays. For this, 20 male wistar rats, which were 6 weeks old, were selected from Shahroud University of Medical Sciences (SHMU) animal house. The rats were kept according to standard conditions described by SHMU. Moreover, the in-vivo experiments were approved ethically based on SHMU procedures (IR.SHMU.REC.1397.047 as ethics code). Rats were categorized randomly in four groups (five rats in each group) and each group was administered based on solution contents as follows: (1) sole solution water (control group), (2) solution water containing pyrite nanoparticles (3) raw TTC solution (50 mg/L and/or 1400 mg/kg of rat body weight) and (4) pyrite/PMS treated TTC solution. All rats were administered via the gavage method by the four determined solutions for seven consecutive days (every once in a day). At the end of day 7, all animals were anesthetized and then heart blood was collected for further biochemical experiments. The hepatotoxicity was evaluated by measuring the plasma levels of liver enzymes including ALT (alanine amino transferase), AST (aspartate amino transferase) and ALP (alkaline phosphatase) using a kit provided by Pars Azmoon (Pars Azmoon Co., IRAN). Nephrotoxicity evaluation was performed by examining the concentration of urea (Ur) and creatinine (Crea) using another analysis kit purchased from Pars Azmoon (Pars Azmoon Co., IRAN). Furthermore, the kidneys and livers were harvested for histopathological examination. The harvested livers and kidneys were incubated in 10 % formalin. After fixation, tissue processing was performed and all produced section stained using haematoxylin and eosin (H&E). Microscopic images were captured using Nikon camera (Nikon D7000 digital SLR camera 3D model).

All the in-vivo assays were performed in triplicate and the results are presented as the average value ± standard deviation of three independent experiments. ANOVA test was used for group comparison and $p < 0.05$ was considered as the statistical significance level.

3. Results and discussion

3.1. Catalyst characterization

The XRD patterns of the fresh pyrite powder and pyrite powder after four successive catalytic reaction cycles are shown in Fig. 2. Identified reflections were in good agreement with the reflections of the pyrite FeS_2 structure, according to the data files of the Joint Committee on Powder Diffraction Standards (JCPDS) database [55,56]: narrow peaks at 2θ of 38.73° and 41.63° are associated to the (2 1 0) and (2 1 1) planes [23,57]; additional peaks positioned at 2θ of 28.15°, 47.8°, 58.1° and 63.7° are ascribed to the (1 1 1), (2 2 0), (2 2 2) and (2 3 0) planes, respectively. XRD results confirmed the high purity of the pyrite sample used in this study, similar to sample derived from the natural material [58,59]. Comparison of the two patterns (before and after reaction) confirmed the absence of structural modification during reaction.

The FTIR spectra of raw pyrite and pyrite after four catalytic reaction cycles are presented in Fig. 3 (wavenumber range from 400 to 4000 cm^{-1}). A moderate broad absorbance band at 3432 cm^{-1} is related to the stretching of hydroxyl vibration groups [60]. Presence of a narrow band at 1640 cm^{-1} is attributed to C═C stretching vibration. The presence of peaks at 601 and 555 cm^{-1} were ascribed to the stretching vibration of the Fe-S bond and asymmetric stretching vibration of Fe—O−OH species [61]. Although a band at 407 cm^{-1} was evidenced for pyrite samples [62], in this study, the band moved to a higher wavenumber, of 478 cm^{-1}, which could be explained by the presence of minor impurities including Cu, Al, and Si elements.

As pyrite has a natural origin, it is necessary to measure the primary elements present in its structure. The elemental analysis of the pyrite particles, measured with the EDAX analyzer, is shown in Fig. 4. Fig. 4 shows that S and Fe were the primary elements found in the pyrite particles with weight percentages of 52.59 % and 44.37 %, respectively. Therefore, S and Fe are the operative elements that are contributing to the oxidation reactions. Moreover, the chemical composition of pyrite was analyzed by XRF, and results are presented in Table 1. SO_3 (66.93 wt %) and Fe_2O_3 (28.57 wt%) were the main compounds present in the pyrite, confirming the EDXS results in Fig. 4.

The surface morphology of pyrite was visualized by SEM (Fig. 5a). The SEM image indicates that pyrite particles are angular and irregular in shape and size. Dense aggregates indicate the absence of porosity in the material. BET surface area of the material is low, 11.6 m^2/g, confirming that the natural pyrite is a low porous material. The pore volume (at $P/P_0 = 0.98$) was calculated to be 0.063 cm^3/g, with calculated average pore size of 1.6 nm.

Fig. 5b shows a typical TEM image of pyrite particles. The dark and bright areas of pyrite nanoparticles in Fig. 5b can be attributed to the

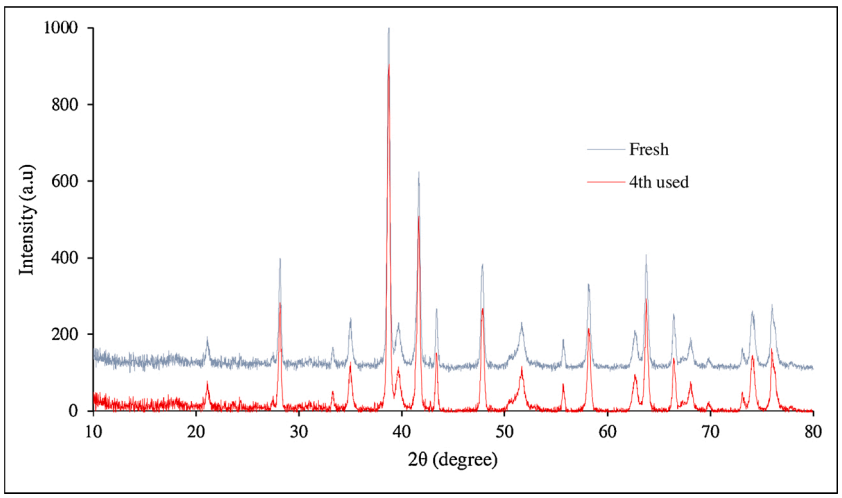

Fig. 2. XRD patterns of fresh pyrite nanoparticles and of used pyrite after four successive catalytic reaction cycles.

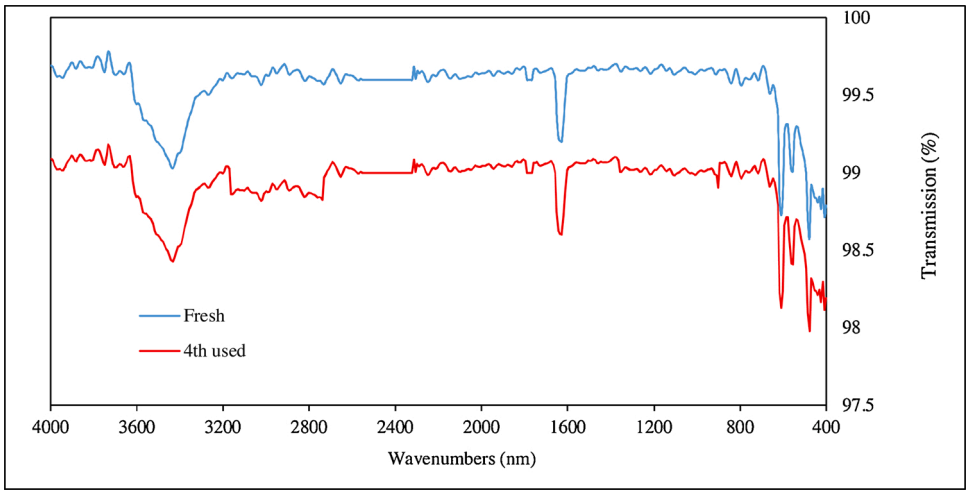

Fig. 3. FTIR spectra of fresh pyrite nanoparticles and of used pyrite after four successive catalytic reaction cycles.

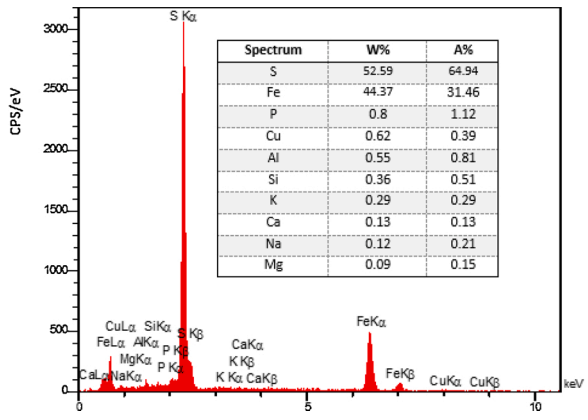

Spectrum	W%	A%
S	52.59	64.94
Fe	44.37	31.46
P	0.8	1.12
Cu	0.62	0.39
Al	0.55	0.81
Si	0.36	0.51
K	0.29	0.29
Ca	0.13	0.13
Na	0.12	0.21
Mg	0.09	0.15

Fig. 4. EDXS analysis of pyrite particles. W% and A% are relative concentrations of detected elements in weight and atomic percentages, respectively.

pyrite particles with high and very thin density, respectively. The size distribution of pyrite nanoparticles induced from the TEM image is shown in Fig. 6: most of the pyrite nanoparticles (nearly 80 %) fall in the range of 30−70 nm. The average particle size of pyrite was about 52.3 nm with a standard deviation (SD) of 12.2 nm. The pyrite sample prepared from mine waste can be considered as a material formed from nanoparticles aggregated together in micro-sized dense objects, displaying a low porosity.

3.2. Catalytic potential of pyrite in activating PMS and PDS

Fig. 7 shows the removal of TTC under various treatment conditions. The TTC removal percentages by pyrite nanoparticles, PDS, and PMS were 3.5 %, 7.5 %, and 16.6 %, respectively. However, by adding PDS and PMS to the pyrite-containing solution, the removal efficiency of TTC increased to 32.5 % and 98.7 %, respectively. These result indicate that both oxidizing agents of PDS and PMS were activated by pyrite nanoparticles and activation efficiency was far more for PMS than for PDS.

The higher removal efficiency of TTC in the pyrite/PMS process than in the pyrite/PDS process can be attributed to the faster and greater oxidation of PMS than PDS by pyrite because of the asymmetric molecular structure of PMS [63]. Similar studies of advanced oxidation, using persulfate radical-based AOPs showed that PMS was an asymmetric compound [1,64]. Also it was found that when PDS was contact with transition metals, it could result in the production of sulfate radicals ($SO_4^{\bullet -}$) [24,25]. Meanwhile, the nonpolar bond of PMS (peroxide bond) was broken by catalytic reactions leading to the generation of both sulfate radicals ($SO_4^{\bullet -}$) and hydroxyl radicals ($OH^{\bullet}$) [64]. The simultaneous presence of these oxidative agents leads to the high

Table 1
Chemical composition of pyrite powders.

Composition	SO_3	Fe_2O_3	SiO_2	Al_2O_3	Na_2O_3	CuO	K_2O	CaO	P_2O_5	MgO	LOI[a]
Composition quantity (wt%)	66.93	28.57	2.91	0.795	0.3	0.14	0.11	0.08	0.02	0.02	17.5

[a] LOI: Lost of ignition.

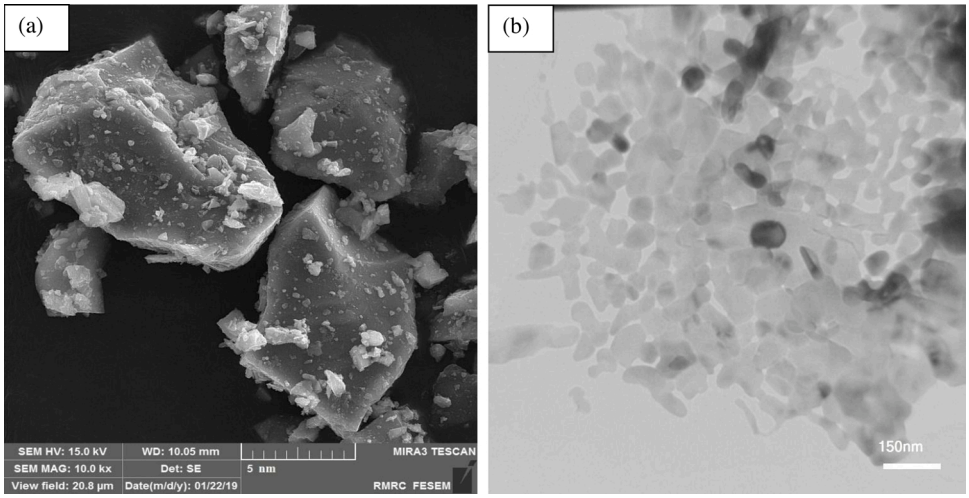

Fig. 5. Representative SEM micrograph (a) and TEM image (b) of pyrite sample.

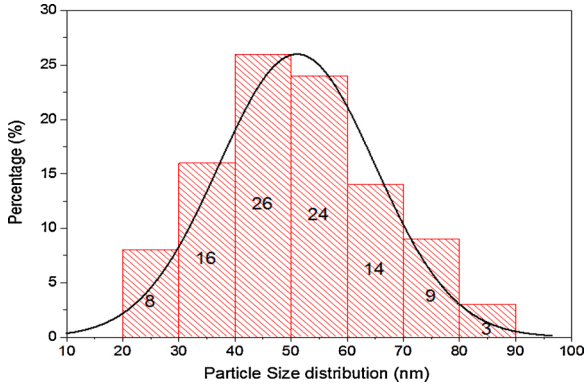

Fig. 6. Particles size distribution histogram of pyrite nanoparticle.

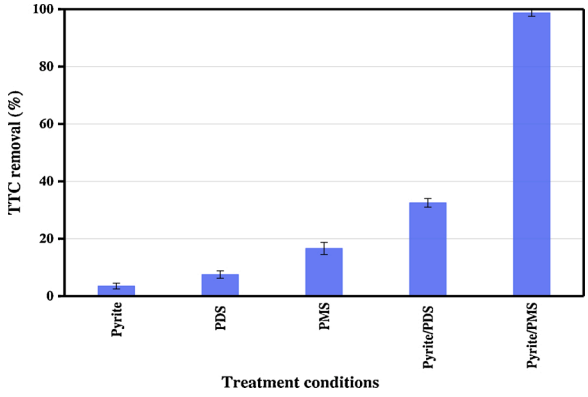

Fig. 7. TTC removal under various conditions (initial TTC concentration: 50 mg/L, catalyst dosage: 1 g/L, PDS/PMS dosage: 1 g/L, solution pH: 4.1, reaction time: 30 min and temperature: 25 °C).

removal of TTC in the pyrite/PMS solution. Several homogeneous and heterogeneous reactions may occur in catalyzing PDS and PMS by pyrite according to following equations [1,22,25]:

$$S_2O_8^{2-} + \equiv Fe(II) \rightarrow SO_4^{\bullet-} + Fe(III) + SO_4^{2-} \quad (4)$$

$$HSO_5^- + \equiv Fe(II) \rightarrow SO_4^{\bullet-} + OH^- + Fe(III) \quad (5)$$

$$2S_2O_8^{2-} + FeS_2 \rightarrow 2SO_4^{\bullet-} + Fe^{2+} + 2SO_4^{2-} + 2S \quad (6)$$

$$2HSO_5^- + FeS_2 \rightarrow 2SO_4^{\bullet-} + 2OH^- + Fe^{2+} + 2S \quad (7)$$

$$2FeS_2 + 7O_2 + 2H_2O \rightarrow 2Fe^{2+} + 4SO_4^{2-} + 4H^+ \quad (8)$$

$$S_2O_8^{2-} + Fe^{2+} \rightarrow SO_4^{\bullet-} + Fe^{3+} + SO_4^{2-} \quad (9)$$

$$HSO_5^- + Fe^{2+} \rightarrow SO_4^{\bullet-} + OH^- + Fe^{3+} \quad (10)$$

However, hydroxyl radicals can be also formed in the solution through the reaction of sulfate radicals with water molecules and hydroxide ions based on following reactions.

$$SO_4^{-\bullet} + H_2O \rightarrow SO_4^{2-} + OH^{\bullet} + H^+ \quad (11)$$

$$SO_4^{-\bullet} + OH^- \rightarrow SO_4^{2-} + OH^{\bullet} \quad (12)$$

Finally, the produced radicals ($SO_4^{\bullet-}$ and $OH^{\bullet}$) react with TTC molecules to produce the degradation products, as could be summarized by Eq (13):

$$SO_4^{\bullet-} + OH^{\bullet} + TTC \rightarrow products \quad (13)$$

In order to confirm the assumptions for the simultaneous formation and active role of each radical $SO_4^{\bullet-}$ and $OH^{\bullet}$ and to demonstrate the relative contribution in the pyrite/PS process, the TTC removal in this process was examined with and without ethanol (as $SO_4^{\bullet-}$ and $OH^{\bullet}$ scavenger) and *tert*-butanol (as $OH^{\bullet}$ scavenger) [9]. Results of this experiment are shown in Fig. 8. The TTC removal efficiency of 98.3 % for the pyrite/PMS process was obtained in the absence of radical scavengers at 30 min reaction time. By adding *tert*-butanol to the

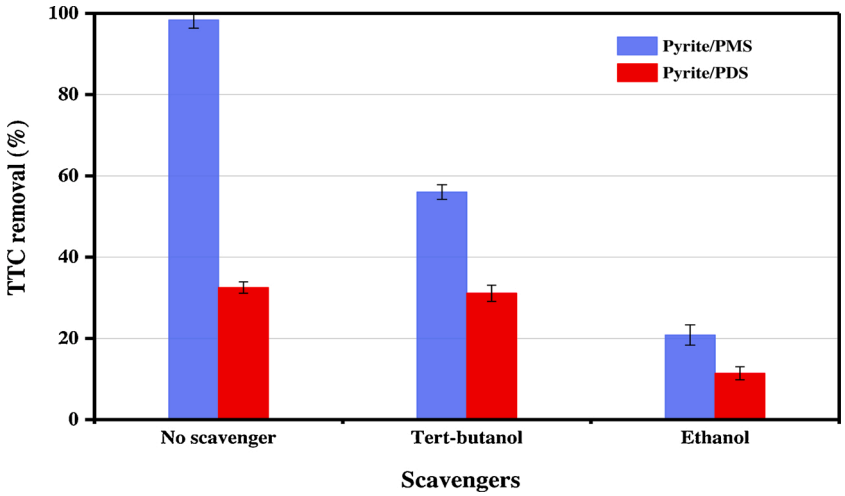

Fig. 8. The influence of radical scavengers on TTC removal in the pyrite/PMS and pyrite/PDS processes (tert-butanol concentration: 0.5 mmol/L, ethanol concentration: 0.5 mmol/L, 50 mg/L initial TTC concentration, 1 g/L catalyst dosage, 1 g/L PMS/PDS, solution pH of 4.1, 30 min reaction time and temperature: 25 °C).

reaction solution, TTC removal decreased to 56 %. However, TTC removal considerably decreased to 20.8 % by the addition of ethanol to the reaction solution. The reaction rates for *tert*-butanol with $OH^{\bullet}$ and $SO_4^{\bullet-}$ are $(3.8-7.6)\times10^8$ M^{-1} s^{-1} and $(4-9.4)\times10^5$ M^{-1} s^{-1}, respectively, the reaction rates for ethanol with $OH^{\bullet}$ and $SO_4^{\bullet-}$ were $(1.2-2.8)\times10^9$ M^{-1} s^{-1} and $(1.6-7.7)\times10^7$ M^{-1} s^{-1}, respectively [1,6,7,65]. According to the reaction rate constants, it can be concluded that the selectivity of $OH^{\bullet}$ for *tert*-butanol is about 1000 times higher than that of $SO_4^{\bullet-}$, while this ratio was significantly lower (by about 100 times) for ethanol. Therefore, a much greater decrease in TTC removal in ethanol compared to *tert*-butanol indicated that both types of $OH^{\bullet}$ and $SO_4^{\bullet-}$ radicals were produced in the pyrite/PMS catalytic process, but $SO_4^{\bullet-}$ played a dominant role in TTC degradation in this process.

Another important point in Fig. 8 is that TTC removal in the pyrite/PDS process in the presence of *tert*-butanol as radical scavengers did not significantly vary compared to the absence of radical scavengers. However, the TTC removal in the presence of ethanol, as specific scavenger of sulfate and hydroxyl radicals [1,7] was significantly reduced by 11.4 %. This result confirms that in the pyrite/PDS process, only $SO_4^{\bullet-}$ is present as active agent in TTC degradation.

3.3. Solution pH and reaction mechanism

The effect of solution pH (3–10) on the removal of TTC, with a constant initial concentration of 50 mg/L, for the adsorption onto pyrite, and the pyrite/PDS and pyrite/PMS processes was investigated. As shown in Fig. 9, the capability of absorbing TTC onto pyrite was very low in the whole pH range and a maximum adsorption of 3.6 % was obtained at pH 4. However, in the pH range tested the TTC removal, different efficiencies for both pyrite/PDS and pyrite/PMS processes were obtained. The maximum TTC removal was attained at acidic pH (<5). As the pH increased above 5, TTC removal significantly reduced. At pH 10, the TTC removal for pyrite/PDS and pyrite/PMS processes were 11.9 % and 55.3 %, respectively. For comparison at pH 4 and 5, the average of TTC removal was 31.5 % and 98 % for pyrite/PDS and pyrite/PMS, respectively. A similar trend was observed by other researchers for the pyrite/PS process [28,66]. The higher removal percentage of TTC at acidic pH compared to the alkaline condition is dependent on several variables, including the concentration of H^+ and OH^- ions, final solution pH, concentration and type of Fe released into the solution, and type of Fe(III) hydroxide complexes formed during the process [67]. High removal at acidic pH in the pyrite/PS processes is often associated to the continuous release of Fe^{2+} from the pyrite surface to the solution, which can react with persulfates, and leads to the production of $OH^{\bullet}$ and $SO_4^{\bullet-}$

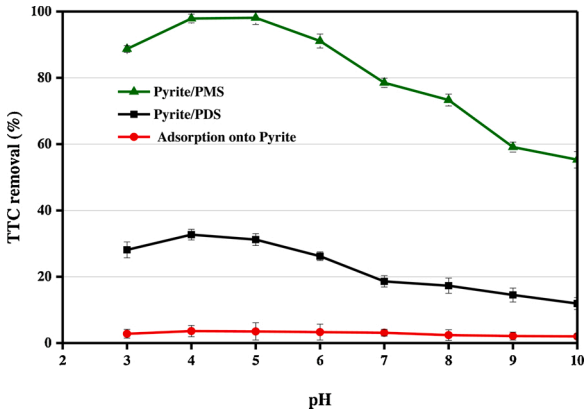

Fig. 9. Effect of solution pH on TTC degradation in the Pyrite/PMS and Pyrite/PDS process, and on TTC adsorption onto Pyrite (Initial TTC concentration: 50 mg/L, Catalyst dosage: 1 g/L, PMS/PDS dosage: 1 g/L, reaction time: 30 min and temperature: 25 °C).

radicals [25,36,66]. It should be noted that PMS/pyrite exhibited a reduction in the performance in pH = 2 (high acidic condition). This phenomenoun can be due to high concentration of hydrogen ions in which they are able to scavenge hydroxyl radicals and sulfate rdicals according to following equations.

$$SO_4^{\bullet-} + H^+ + e^- \rightarrow HSO_4^{\bullet-} \quad (14)$$

$$HO^{\bullet} + H^+ + e^- \rightarrow H_2O \quad (15)$$

An increase in pH value up to alkaline conditions causes the precipitation of hydroxide complexes of Fe(II) and Fe(III) such as $Fe(OH)_2$, $Fe(OH)_3$, and to the formation of $Fe_2(OH)_2^{4+}$ in the reaction solution [67]. These species reduce the activation of persulfates since they display lower catalytic activity than Fe^{2+} [25]. Moreover, these hydroxide complexes can also deposit on the catalyst surface, preventing the release of Fe^{2+} from the catalyst surface to the reaction solution, and decrease the activation of persulfates by Fe(II) [25,66]. In case of PMS based process, it has been reported that PMS is decomposed into sulfate and water molecules at high alkaline conditions. Moreover, pKa of PMS is 9.4 in which SO_5^{2-} is dominated at pH > 9.4 that its activation is difficult due to lack of O—H bond. Hence, alkaline conditions decrease the generation of free radicals through reduction of persulfate species.

$$HSO_5^- + OH^- \rightarrow SO_4^{2-} + \frac{1}{2} O_2 + H_2O \quad (16)$$

Another factor to explain the increased TTC removal at acidic pH could be the higher generation of $SO_4^{\bullet-}$ as the dominant agent, rather than $OH^{\bullet}$. In contrast, in alkaline conditions $OH^{\bullet}$ was produced at a higher rate than $SO_4^{\bullet-}$ and can reacted with $SO_4^{\bullet-}$ to produce HSO_4^- as inert anion (Eq. 17) [25,67]. Therefore, the concentration of $SO_4^{\bullet-}$ in the solution, which we previously identified as the dominant radical for the TTC degradation, was reduced, leading to the decreased catalytic activity.

$$SO_4^{\bullet-} + OH^{\bullet} \rightarrow HSO_4^- + \frac{1}{2} O_2 \quad (17)$$

Fig. 9 also shows a considerable TTC removal by the pyrite/PMS process even at higher pH values. As mentioned previously, an important mechanism involved in TTC removal in the pyrite/PS process is the interaction between Fe^{2+} and PS at acidic pH. However, as demonstrated in Fig. 9, the TTC removal at alkaline pH of 10 still remained 55.3 %. This high removal could be due to the generation of $OH^{\bullet}$ by reaction of OH^- with $SO_4^{\bullet-}$ (Eq. (12)) [25,66].

In order to confirm the assumptions made about the reaction mechanism of the production of reactive radical species in the TTC degradation process, the concentration of Fe^{2+} and total dissolved Fe of the solution in the pyrite/PMS process and the final pH of the reaction solution were monitored (Fig. 10). To obtain more accurate information about the final destination of Fe released into the solution and the final pH of the solution, the reaction time was increased to 60 min. As shown in Fig. 10, with increasing pH from 3 to 10, the concentrations of Fe^{2+} and total dissolved iron was reduced by 0.033 mg/L (from 0.042 to 0.009 mg/L) and by 0.52 mg/L (from 0.65 to 0.13 mg/L), respectively. This phenomenon shows that the largest and continuous release of Fe from the pyrite surface to the solution occurs typically under acidic conditions (compared to alkaline) leading to high degree of PMS activation and generation of more active radical species. However, at alkaline pH, the release of Fe from the pyrite surface to the bulk solution reduced and subsequent catalytic reactions were decreased due to reasons that were mentioned previously, such as deposition of ferrous hydroxides on the pyrite surface [36,67].

Fig. 10 also shows that the final pH of the reaction solution reduced to 2.9, 3.6, 4.1, and 5.3 for initial solution pH of 3, 5, 7, and 9, respectively, during the 60 min reaction time. At an initial pH of 10, the decrease to a pH of 8.1 was relatively less pronounced as compared with an initial pH of 7 and 9. The considerable reduction of the final pH of the reaction solution during the 60 min reaction time explains the assumptions made about the reaction mechanism and production of active radical species with the release of Fe from the pyrite surface to the solution and the reaction with PMS. In this regard, the considerable decrease in the final pH of the reaction solution could be due to the oxidation of pyrite in the reaction solution by H_2O molecules, the release of Fe^{2+} and Fe^{3+} from the pyrite surface and the production of H^+ in solution (Eq. (18)) [12,24]. Also, the reaction between $SO_4^{\bullet-}$ and the alkaline agent OH^- and H_2O can lead to the consumption of OH- and production of H^+ (Eqs. (11) and (12)). These phenomena lead to the spontaneous reduction of the solution pH, to optimal acidic conditions, after adding reaction agents (pyrite and PMS) and resulted in relatively high TTC removal even at initial basic pH.

$$FeS_2 + 14Fe^{3+} + 8H_2O \rightarrow 15Fe^{2+} + 2SO_4^{2-} + 16H^+ \quad (18)$$

Since the pyrite/PMS process showed considerable higher TTC removal than the pyrite/PDS process in the whole pH range from 3 to 10, the catalytic activity of pyrite and the effect of operational parameters were studied in the pyrite/PMS process. Moreover, as the maximum TTC removal was obtained at initial pH levels 4–5, the natural TTC pH solution of 4.1 was selected for further experimental runs.

3.4. Kinetics of catalytic activity of pyrite nanoparticles in the pyrite/PMS process

The catalytic activity of pyrite nanoparticles was examined on the degradation and mineralization of 50 mg/L TTC. Fig.11a shows the TTC degradation in the sole PMS and pyrite/PMS processes, as well as the catalytic performance of the pyrite nanoparticles at different reaction times under similar conditions.

As noted earlier, the TTC adsorption by pyrite was low (maximum adsorption of 3.6 % during 30 min reaction time, Fig. 7). Accordingly, sole PMS and pyrite/PMS processes were selected for kinetic studies. As shown in Fig. 11a, by increasing the reaction time from 1 to 45 min, the TTC degradation by sole PMS process increased from 2.6%–26.3%, respectively. In the pyrite/PMS process, TTC degradation was much

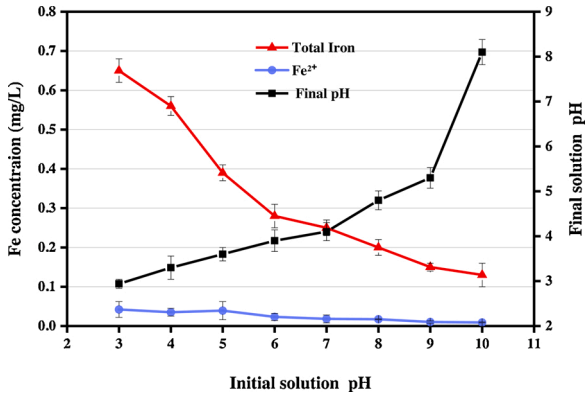

Fig. 10. Changes in Fe^{2+}, total Fe ions concentration and final pH solution in the pyrite/PMS process according to the initial solution pH.

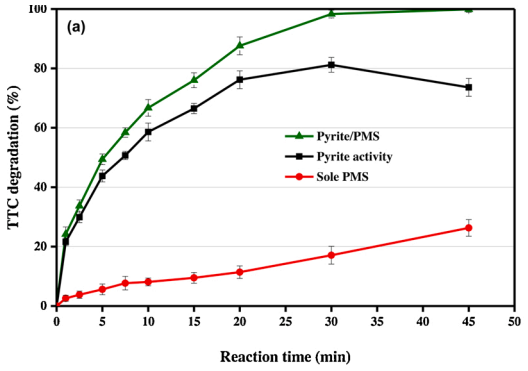

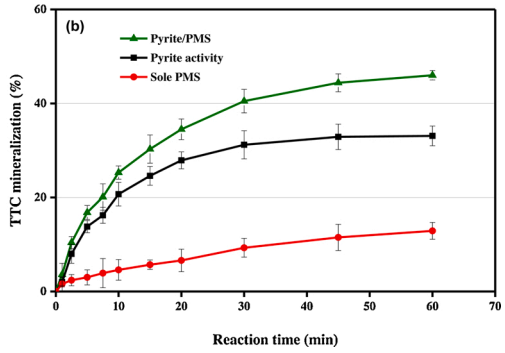

Fig. 11. Catalytic activity of pyrite nanoparticles for the degradation (a) and mineralization (b) of TTC as a function of reaction time in the sole PMS and Pyrite/PMS process (Initial TTC concentration: 50 mg/L, Catalyst dosage: 1 g/L, PMS concentration: 1 g/L, Solution pH: 4.1 and temperature: 25 °C).

higher and reached 24.2 % already after a reaction time of 1 min. Furthermore, by increasing the reaction time to 30 min, the TTC degradation increased considerably and reached 98.3 %. Complete TTC degradation was obtained in 45 min. The catalytic activity of the process was also elevated with increased reaction time, reaching about 21.6 % after 1 min and a maximum of 81.2 % at 30 min reaction time. Fig. 11b illustrates the TTC mineralization by the pyrite/PMS process at different reaction times, based on TOC reduction. Accordingly, the treatment with the individual PMS process led to 1.6 % TOC reduction at 1 min reaction time, which increased to 12.9 % by increasing the reaction time to 60 min. However, by increasing the reaction time from 1 to 60 min, the TOC reduction increased from 3.6%–46% in the pyrite/PMS process. The maximum catalytic activity of the pyrite/PMS process in TTC mineralization was 33 % at 60 min reaction time. These results indicate that although the pyrite/PMS process had a high capability to completely degrade TTC from aqueous solutions, it was not capable to completely mineralize TTC even at higher reaction times. However, the results show a significantly higher TTC degradation and mineralization capability compared to the sole PMS process. Since the maximum catalytic activity of the pyrite/PMS process for TTC degradation was obtained at 30 min reaction time, the examination of other process variables was set at this reaction time.

To better understand the catalytic activity of pyrite nanoparticles in PMS activation for TTC degradation, kinetic studies on TTC degradation and mineralization in sole PMS and pyrite/PMS processes were performed and results were modeled using the pseudo-first-order (PFO) reaction model, which is calculated by the following equations:

$$r_1 = -\frac{dC}{dt} = k_{obs} C \tag{19}$$

$$\ln\left(\frac{C_t}{C_0}\right) = -k_{obs} t \tag{20}$$

where, C_0 and C_t refers to the concentrations of TTC and TOC at the time 0 (initial) and time t (final), respectively, and the k_{obs} refers to the PFO reaction rate constant. According to the findings, the PFO model was well fitted ($R^2 > 0.95$) to the results of the degradation and mineralization experiments presented in Fig. 11. Data on the kinetics of TTC degradation and mineralization are summarized in Table 2. Based on the results, TTC degradation rate in the pyrite/PMS process ($r_{pyrite/PMS}$ =4.331 mg TTC /L. min) was approximately 12 times higher than in the sole PMS process ($r_{sole\ PMS}$ =0.365 mg TTC /L. min). In this regard, TTC mineralization rates in the sole PMS and pyrite/PMS process were 0.225, and 1.37 mg TOC /L. min, respectively. These data show that the addition of pyrite to the PMS process significantly increased the process performance from both TTC degradation and TTC mineralization aspects.

3.5. Effect of pyrite dosage and PMS concentration in the pyrite/PMS process

Since determining the optimum concentration of reactive agents in catalytic processes is important from an economic point of view, TTC removal was investigated at various concentrations of pyrite and PMS in the pyrite/PMS process. Fig. 12 shows the effect of pyrite dosage ranging from 0.02 to 2 g/L on TTC removal in the pyrite/PMS process. By

Table 2
Kinetics of TTC degradation and mineralization for sole PMS and Pyrite/PMS processes.

Process	Sole PMS	Pyrite/PMS $\frac{r_{Pyrite/PMS}}{r_{Sole\ PMS}}$
	R^2 K_{obs} $r_{Sole\ PMS}$	R^2 K_{obs} $r_{Pyrite/PMS}$
Degradation	0.9601 0.0073 0.365	0.9937 0.0860 4.331 11.78
Mineralization	0.9706 0.0045 0.225	0.9706 0.0274 1.37 6.08

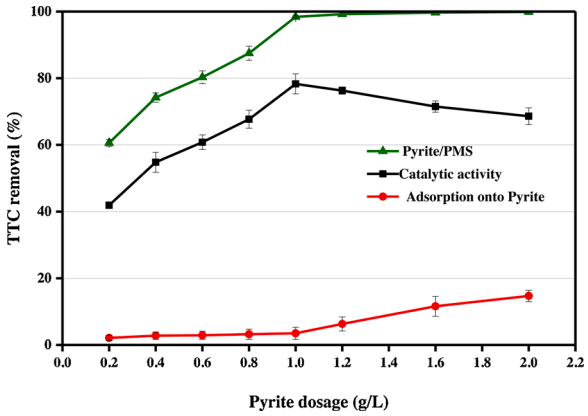

Fig. 12. Effect of initial pyrite dosage on TTC removal using adsorption onto pyrite and pyrite/PMS processes (reaction conditions: pH: 4.1, TTC concentration: 50 mg/L, 30 min reaction time, temperature: 25 °C and PMS concentration: 1 g/L).

increasing the pyrite dosage from 0.02 to 2 g/L, TTC adsorption on pyrite increased smoothly from 2.1%–14.7%. The slow increase in TTC adsorption might be due to the low specific surface area of pyrite used in this study (11.6 m^2/g). Therefore, the adsorption mechanism cannot be considered as an effective process for the TTC removal by pyrite. Increased pyrite dosage in the pyrite/PMS process showed another trend and higher removal was attained by increasing the pyrite dosage. TTC removal >98 % in the pyrite/PMS process was obtained since a pyrite dosage of 1 g/L. The considerable increase in TTC

removal by increasing the pyrite dosage in the pyrite/PMS process might be a result of a higher Fe^{2+} release from the surface of the catalyst to the reaction solution, further activating PMS, and finally resulting in a higher production of $OH^{\bullet}$ and $SO_4^{\bullet-}$ radicals [36,64]. The optimal catalytic activity for the pyrite/PMS process was obtained at 1 g/L pyrite dosage, which was considered in the next pyrite/PMS experiments. Moreover, the results showed that excess pyrite (more than 1 g/L) did not demonstrate inhibition effect on the efficiency of TTC removal which can be an advantage for catalytic processes.

The effect of various concentrations of PMS (0.2–2 g/L) on the TTC removal was investigated in sole PMS and pyrite/PMS processes. As shown in Fig. 13, with increasing PMS concentrations from 0.2 to 2 g/L, the TTC degradation increased gradually and continuously from 8.5%–36.4% in the sole PMS process. Therefore, the sole PMS process was not capable for effective TTC degradation. TTC degradation in the sole PMS process could be due to the direct attack of HSO_5^-, as the main species from PMS, in acidic solution (Eq. 6). By adding 1 g/L pyrite to the reaction solution containing 0.2 g/L PMS, the TTC degradation considerably increased to 60.8 %. This indicated that pyrite is an effective

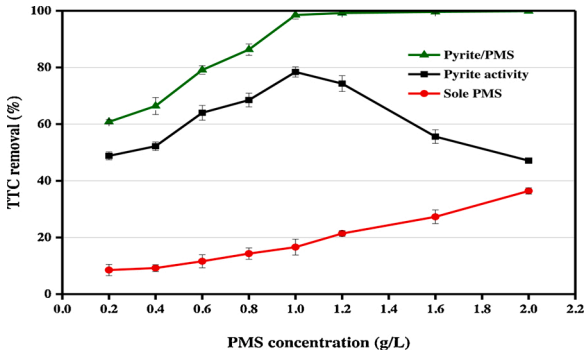

Fig. 13. Effect of initial PMS concentration on TTC removal using sole PMS and pyrite/PMS processes (reaction conditions: TTC concentration: 50 mg/L, pH: 4.1, reaction time: 30 min, temperature: 25 °C and pyrite dosage: 1 g/L).

activator to release Fe^{2+} for production of $SO_4^{\bullet-}$ [64]. TTC degradation > 98 % was obtained at a concentration of 1 g/L PMS. As the maximum catalytic activity of the pyrite/PMS process (78 % TTC degradation) was obtained at 1 g/L PMS, this concentration was considered as the optimal concentration of PMS for further experiments in the study. Liang et al. [24] conducted a research into the removal of MTBE in aqueous solutions using the pyrite/PDS process and found that complete MTBE degradation was obtained at a pyrite dosage of 3 g/L, an $Na_2S_2O_8$ concentration of 5 g/L, and a reaction time of 4 h. The key role of pyrite in the activation of PMS to produce oxidative radicals was also confirmed in this study.

3.6. The effect of solution temperature and initial TTC concentration on process performance

Solution temperature and initial TTC concentration are factors which can influence the catalytic performance of the process. Therefore, the pyrite/PMS process was investigated at various initial TTC concentrations, from 25 to 500 mg/L, with 1 g/L of pyrite and PMS concentration of 1 g/L, at three specific temperatures (15-25−40 °C). Fig. 14 shows the TTC removal at varying initial TTC concentrations at various temperatures. Both the temperature and initial concentration affected TTC removal in the pyrite/PMS process. By increasing the initial TTC concentration, the TTC removal decreased for the three temperatures studied. According to the constant quantity of generated oxidizing agents in the pyrite/PMS process at determined conditions, the ratio of oxidizing agents to the TTC molecules decreased by enhancing the TTC concentration, mechanically resulting in the reduction of removal percentage. In addition, an increase in TTC molecule quantity in a determined volume of the reaction solution, makes PMS directly to react with the TTC molecules, instead of reacting with pyrite molecules. Therefore, this parallel reaction prevents the production of active $OH^{\bullet}$ and $SO_4^{\bullet-}$ radicals [10,68] and can result in a depressed process efficiency.

Fig. 14 also shows that the TTC removal increased with increasing temperature whatever the TTC concentration. Increased TTC removal with increasing temperature at a certain concentration could be due to the increase in radical concentration in solution. According to the Arrhenius law [16], as the temperature increases, the production of active radicals such as $OH^{\bullet}$ and $SO_4^{\bullet-}$ increases in catalytic processes. It has also been shown that an increase of solution temperature could increase the mass transfer and enhance the diffusion coefficients [6]. Therefore, when the temperature was enhanced, the TTC molecules diffusion rates and mass transfer along with the effective collision between the TTC molecules in the bulk solution and oxidative agents could be increased. So, TTC removal will be improved. In addition, O—O bond of PMS is homolytically cleaved at higher temperature to generate free radicals. Whole these phenomenon are in favor of the TTC degradation rate when the reaction temperature increases.

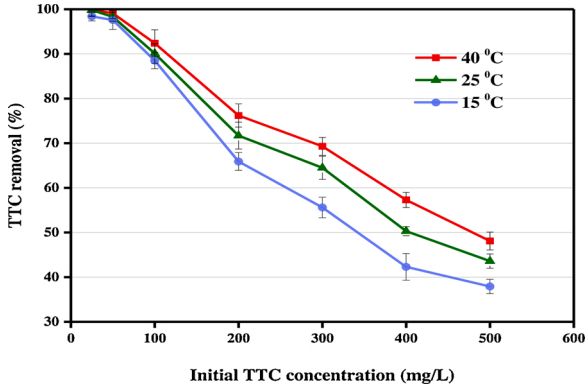

Fig. 14. The influence of solution temperature on TTC removal at various TTC concentrations in the pyrite/PMS process (reaction conditions: 50 mg/L initial TTC concentration, pH 4.1, 1 g/L PMS, 1 g/L pyrite dosage, 60 min reaction time).

3.7. Comparison with pyrite from other origin as catalyst in the activation of persulfates (PDS/PMS)

The performance of other pyrite samples, non-waste mineral and synthetic ones, as catalyst for the activation of PS and for removal of organic pollutants in aqueous solution, was compared with the present study and the results are presented in Table 3. The comparison of degradation efficiency and reaction time (columns 4 and 5, Tabels 2) revealed that the used pyrite from mine waste has similar and/or better performance characteristics compared to non-waste mineral pyrite and synthetic pyrite, indicating that the waste mine pyrite is a promising effective catalyst in the activation of PS.

3.8. Effect of inorganic ions on TTC removal in the pyrite/PMS process

Generally, inorganic ions are major components in natural water resources, and they can affect the oxidation rate of organic compounds [25]. Studies have then shown that the presence of some coexisting ions had adverse effect on the degradation rates of water organic pollutants in AOPs [75,76]. Therefore, the removal efficiency of TTC by the pyrite/PMS process was investigated in the presence of some common ions including CO_3^{2-}, HCO_3^-, Cl^-, NO_3^- and SO_4^{2-}. As illustrated in Fig. 15, TTC degradation was not considerably influenced in the presence of Cl^- and NO_3^-. Whereas, SO_4^{2-}, HCO_3^- and CO_3^{2-} had a much more significant influence following the order: $CO_3^{2-} > HCO_3^- > SO_4^{2-}$. The adverse effect of inorganic ions could be explained as follows: The presence of SO_4^{2-} may decrease PMS decomposition due to higher ionic strength of SO_4^{2-} than $SO_4^{\bullet-}$ [25]. Moreover, the reaction reduction potential of $SO_4^{\bullet-}$ will be reduced in the presence of SO_4^{2-} $\left(E^0_{(SO_4^{\bullet-}/SO_4^{2-})}\right)$. Based on Nernst equation (Eq. (21)) [77], it can be concluded that the oxidation/reduction potential of $SO_4^{\bullet-}/SO_4^{2-}$ could be affected by the concentration of SO_4^{2-} [78]. According to generation processes of $SO_4^{\bullet-}$ radicals and hypothesizing that the TTC degradation resulted in depletion of $SO_4^{\bullet-}$ radicals (Eq. 22), presence of SO_4^{2-} ions in the suspension decreased the potential of $E^0_{(SO_4^{\bullet-}/SO_4^{2-})}$ which straightly reduced the TTC degradation.

$$E^0_{(SO_4^{\bullet-})} = E^0_{(SO_4^{\bullet-}/SO_4^{2-})} + \frac{RT}{zF}\ln\frac{SO_4^{\bullet-}}{SO_4^{2-}} \quad (21)$$

$$SO_4^{\bullet-} + e^- \rightarrow SO_4^{2-} \quad (22)$$

A considerable inhibition effect on TTC degradation was measured for HCO_3^- and CO_3^{2-} ions. This could be explained by the scavenger effect of HCO_3^- and CO_3^{2-} on $OH^{\bullet}$ and $SO_4^{\bullet-}$ radicals, as written in (Eqs. (23) and (24)) [25]. Moreover, the presence of HCO_3^- and CO_3^{2-} ions results in initial solution pH increase via hydrolysis, and thus the production of $OH^{\bullet}$ and $SO_4^{\bullet-}$ decreased, leading to a reduction of TTC degradation (Fig. 9) [77]. Although other less active radicals including $CO_3^{\bullet-}$ could be produced from the reactions of HCO_3^- and CO_3^{2-} with $SO_4^{\bullet-}$ and $OH^{\bullet}$, it has a low oxidation potential (E° =1.7 V) and lower degradation capacity of TTC, resulting in a decrease in TTC removal [79]. According to reported studies, the reaction rate constants of TTC with $OH^{\bullet}$ and $SO_4^{\bullet-}$ were found to be 6.0×10^9 M^{-1} s^{-1} [11,80] and 1.4×10^{10} M^{-1} s^{-1} [81], respectively, while the reaction rate constants of TTC with $CO_3^{\bullet-}$ were reported 2.9×10^8 M^{-1} s^{-1} [82].

$$HCO_3^- + SO_4^{\bullet-} \rightarrow CO_3^{\bullet-} + SO_4^{2-} + H^+ \quad (23)$$

$$CO_3^{2-} + OH^{\bullet} \rightarrow OH^- + CO_3^{\bullet-} \quad (24)$$

In addition, PMS can directly react with bicarbonate ions and,

Table 3
Comparison of removal efficiency of water organic pollutants using pyrite for the activation of persulfates (PMS/PDS).

Process	Shape and purification method of pyrite	Pollutant(s)	Experimental conditions	Maximum degradation efficiency at optimum condition	K_{obs} (min^{-1})	Fitted model	Correlation coefficient (R^2)	Ref.
Pyrite/PS	The nano size particles were rinsed with ethanol and deionized water (50/50) for 3 times	TTC	• pH: 3–10 • Reaction time: 0–45 min • Initial contaminant concentration: 25–500 mg/L • Pyrite loading: 0.2–2 g/L • PMS/PDS: 0.2–2 g/L • Temperature: 15–40 °C	• 98 % @ 45 min	0.086	PFO	99.37	Present study
Pyrite/PDS	Microparticles supplied from sulfure-polymetallic, cleaned with 0.1 M HNO_3	Rhodamine B	• pH: 2–11 • Reaction time: 0–120 min • Initial contaminant concentration: 19.6 mg/L • Pyrite loading: 1 g/L • PMS loading: 2–10 mM • Temperature: 25 ± 1 °C	• 98 % @ 120 min	0.0304	PFO	0.987	[58]
Pyrite/PDS	Microparticles supplied from sulfure-polymetallic, cleaned with 0.1 M HNO_3	2,4-diclorophenol	• pH: 4–10 • Reaction time: 0–120 min • Initial contaminant concentration: 10 mg/L • PMS concentration: 0.5–2 mM • pyrite dosage: 0.25–1.5 g/L • Temperature: room	• 71.3 % @ 120 min	Not reported	Not reported	Not reported	[69]
Pyrite/PDS	FeS_2 was synthesized using a one-step hydrothermal method	Atrazine	• pH: 7 • Reaction time: 0–90 min • Initial contaminant concentration: 20 mg/L • Pyrite loading: 4.2 mM • Sodium persulfate: 3 mM • Temperature: 25 °C	• 100 % @ 45 min	Not reported	Not reported	Not reported	[70]
Pyrite/PDS	Pyrite ground was milled by a hammermill, and sieved to obtain fine particles with a diameter of < 150 μm	Ethylthionocarbamate	• pH: 3–11 • Reaction time: 0–180 min • Initial contaminant concentration: 0.1 mM • Pyrite loading: 0.1–1 g/L • Sodium persulfate: 0.012–0.12 g/L • Temperature: 10–50 °C	• 96.64 % @ 180 min	Not reported	Not reported	Not reported	[23]
Pyrite/PDS	Microparticles supplied from Dabaoshan sulfur-polymetallic mines and grinded to 20–200 mesh	p-chloroaniline	• pH: 3–11 • Reaction time: 0–250 min • Initial contaminant concentration: 0.1 mM • Pyrite loading: 0.1–1 g/L • Sodium thiosulfate pentahydrate loading: 0.5 mM • Temperature: 10–50 °C	• 100 % @ 60 min	Not reported	Not reported	Not reported	[36]

(*continued on next page*)

Table 3 (*continued*)

Process	Shape and purification method of pyrite	Pollutant(s)	Experimental conditions	Maximum degradation efficiency at optimum condition	K_{obs} (min^{-1})	Fitted model	Correlation coefficient (R^2)	Ref.
Pyrite/PDS	Grounded pyrite passed through 200 mesh sieve. It was washed with a 1 M HCl acid solution to remove impurities and then rinsed with RO water until the pH of the supernatant was stable at ~6.5.	methyl tertbutyl ether (MTBE)	• Initial pH: 5.5–5.8 • Reaction time: 4–12 h • Initial contaminant concentration: 60 mg/L • Pyrite loading: 1–5 g/L $Na_2S_2O_8$ loading: 1–5 g/L • Temperature: 20 °C	• 100 % @ 4 h	0.61–1.97	PFO	0.99	[24]
Pyrite/PDS	Pyrite chips were were pulverized and sieved to obtain fine particles with diameters smaller than 149 μm (−100 mesh).	2,4-dinitrotoluene	• Initial pH: 5.6–6.6 • Reaction time: 0–180 min • Initial contaminant concentration: 50 mg/L • Pyrite loading: 0.2–1 g/L • $Na_2S_2O_8$ concentration: 250 mg/L	• 100 % @ 10 min	6.9×10^{-2}	PFO	0.961	[71]
Pyrite/PDS	Nanoparticles, washed with ultrapure water	Acetaminophen	• pH: 4–10 • Reaction time: 0–360 min • Initial contaminant concentration: 50 mg/L • pyrite dosage: 2 g/L • Peroxydisulfate: 5 mM	• 96.6 % @ 180 min	Not reported	Not reported	Not reported	[72]
Pyrite/PDS	Microparticles, rinsed with distilled water, 50 % HCl and ethanol	Tris(2-chloroethyl) phosphate (TCEP)	• pH: 3–11 • Reaction time: 0–120 min • Initial contaminant concentration: 2 mg/L • Persulfate concentration: 0.5–5 mM • pyrite dosage: 0.03–0.5 g/L • Temperature: ambient	• 100 % @ 120 min	$-(3.23 \pm 0.33) \times 10^{-2}$	PFO	0.9401	[73]
Pyrite/PDS	Pyrite powder washed with 95 % ethanol, 1 M HNO3 and deionized water, successively	Orange G	• pH: 3–9 • Reaction time: 0–60 min • Initial contaminant concentration: 100 μM • PDS concentration: 5 mM • pyrite dosage: 0.25–2 g/L • Temperature: 30 ± 0.5 °C	• 100 % @ 60 min	Not reported	Not reported	Not reported	[74]

peroxymonocarbonate may be formed (Eq. (25)), therefore, the generation of free radicals from PMS is significantly reduced.

$$HSO_5^- + HCO_3^- \rightarrow HCO_4^- + HSO_4^- \quad (25)$$

Results of the inorganic ions experiments in this research are somehow in agreement with those of other sulfate radical-based AOPs studies. It should be noted that a significant attention should be considered for scale up of pyrite/PMS process when a real water or wastewater is treated.

3.9. Catalyst reusability

The reusability of the nano-pyrite particles was evaluated during fourth cycles under identical experimental conditions as follows: 1 g/L PMS, pH 4.1, 1 g/L pyrite dosage, 50 mg/L initial TTC concentration, temperature: 25 °C and 30 min reaction time. For this purpose, the used pyrite nanoparticles were filtered from the suspension solution at the end of each cycle, washed, and dried at 60℃ in a sealed quartz tube to prevent further oxidation in air and, then, were used in the next cycle. TTC removal for these fourth successive cycles is presented in Fig. 16. It was found that high TTC removal is retained in all reaction cycles. The TTC removal for fresh pyrite nanoparticles was about 98.3 %. After fourth consecutive cycles of reusing pyrite, the percentage of TTC removal was almost not affected and remained above 90 %. The progressive slight decrease observed between each cycle could partly originate from the pyrite weight fluctuation in each cycle (due to the

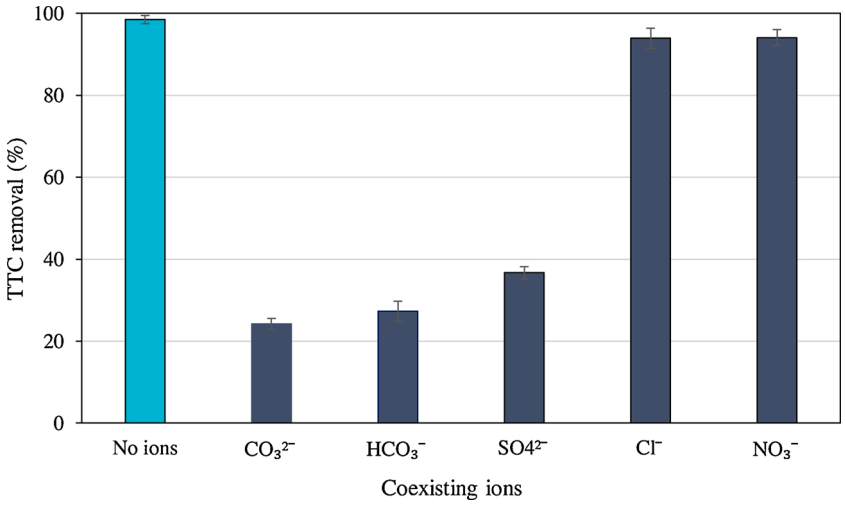

Fig. 15. Influence of various ions on TTC degradation efficiency in the Pyrite/PMS process (reaction conditions: 50 mg/L TTC, pH 4.1, 1 g/L PMS, 1 g/L pyrite dosage, temperature: 25 °C and 30 min reaction time).

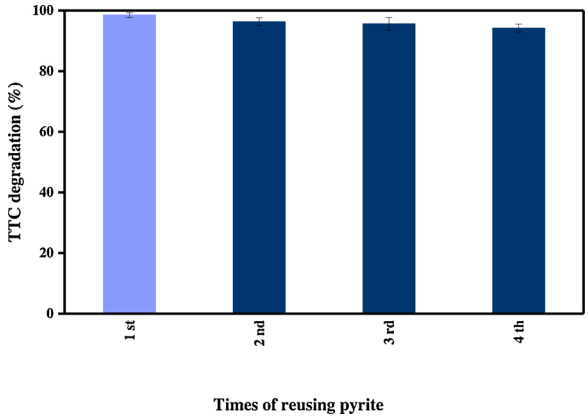

Fig. 16. The reusability of pyrite for TTC degradation in the pyrite/PMS (reaction conditions: 50 mg/L TTC, pH 4.1, 1 g/L PMS, 1 g/L pyrite dosage, temperature: 25 °C and 30 min reaction time).

recovery / separation steps). Analyses of catalyst after reaction (by XRD and FTIR), and comparison with fresh pyrite sample evidence the absence of consequent pyrite structural change (Figs. 3 and 4).

3.10. Effect of treatment in the pyrite/PMS on in-vivo toxicity of TTC

The in-vivo toxicity of raw and pyrite/PMS TTC treated solutions, under optimum conditions, was examined using hepatotoxicity and nephrotoxicity assays. Moreover, the effect of raw water solution and pyrite nanoparticles on in-vivo toxicity were considered, separately. The hepatotoxicity and nephrotoxicity results obtained from the biochemical assays demonstrated that the liver and kidney function was significantly ($p < 0.03$) disturbed by the raw TTC solution. As shown in Fig. 17, all liver function tests including ALT, AST and ALP display a significant increase with raw TTC solution compared to the other three groups (water, water + pyrite, pyrite/PMS treated). The concentrations of ALT, AST and ALP for the rats that were exposed to pure water solution were 53, 131.8 and 273 international unit (IU), respectively; in contrast they were about 77, 183 and 585 IU for those induced with raw TTC solution. The concentration of ALT and AST were not increased in the presence of pyrite nanoparticles in the water solution and in the pyrite/PMS TTC treated solution, indicating pyrite nanoparticles as a natural material, had no hepatotoxic effect. Although the concentration of ALP increased from 273 IU to 345 and 315 IU for the water solution containing pyrite nanoparticles and pyrite/PMS TTC treated solution, respectively, these increases were not considered as significant ($p > 0.05$). Moreover, the concentration of urea and creatinine, as kidney function tests, also increased for those induced with raw TTC solution (Fig. 17), but the increases were not significant ($p > 0.05$).

The histopathological assays show that raw TTC solution had acute toxicity on liver and kidney tissues. As observed in Fig. 18 (red arrows), inflammation was observed for liver tissue. In addition, small size glomeruli, with loss of brush border in proximal convoluted tubules were observed in kidney tissue (Fig. 19, red arrows). Furthermore, in both proximal and distal convoluted tubules, vacuoles and desquamating cells were detected. However, no liver and kidney abnormality was detected for the other three groups.

In conclusion, the biochemical and histopathological assays clearly demonstrated that raw TTC solution had a toxic effect on liver and kidney function. Treating the TTC solution with the pyrite/PMS process clearly decreased the toxicity effect. Hence, the pyrite/PMS process could be considered as a potentially helpful technique for detoxification of polluted water.

4. Conclusions

In this study, the catalytic performance of mine waste pyrite nanoparticles in activating peroxydisulfate (PDS) and peroxymonosulfate (PMS) compounds was evaluated for the removal of tetracycline (TTC), as an emerging water contaminant. The maximum pyrite activity of TTC degradation and mineralization was 81.2 % and 33.1 %, respectively, in the pyrite/PMS process at pH = 4.1, 1 g/L pyrite, 1 g/L PMS dosage, 50 mg/L initial TTC concentration, 30 min reaction time, and temperature of 25 °C. It was revealed that $SO_4^{\bullet-}$ had a dominant role in the TTC removal reaction in the pyrite/PMS process. Presence of SO_4^{2-}, HCO_3^- and CO_3^{2-} ions in water had a considerable inhibiting effect on TTC degradation (62%–74.5% when compared to the ion-free reaction). Presence of pyrite in the water solution was also verified to have not significant toxic effect. In conclusion, mine waste pyrite mineral can be considered as a non-toxic catalyst to activate PMS in the pyrite/PMS process, resulting in an effective degradation, intermediate mineralization and detoxification of polluted water.

Ethical approval

The Ethics Committee of Shahroud University of Medical Sciences has approved the project in accordance with the tenets of the Helsinki Declaration and the national ethical guideline for medical research.

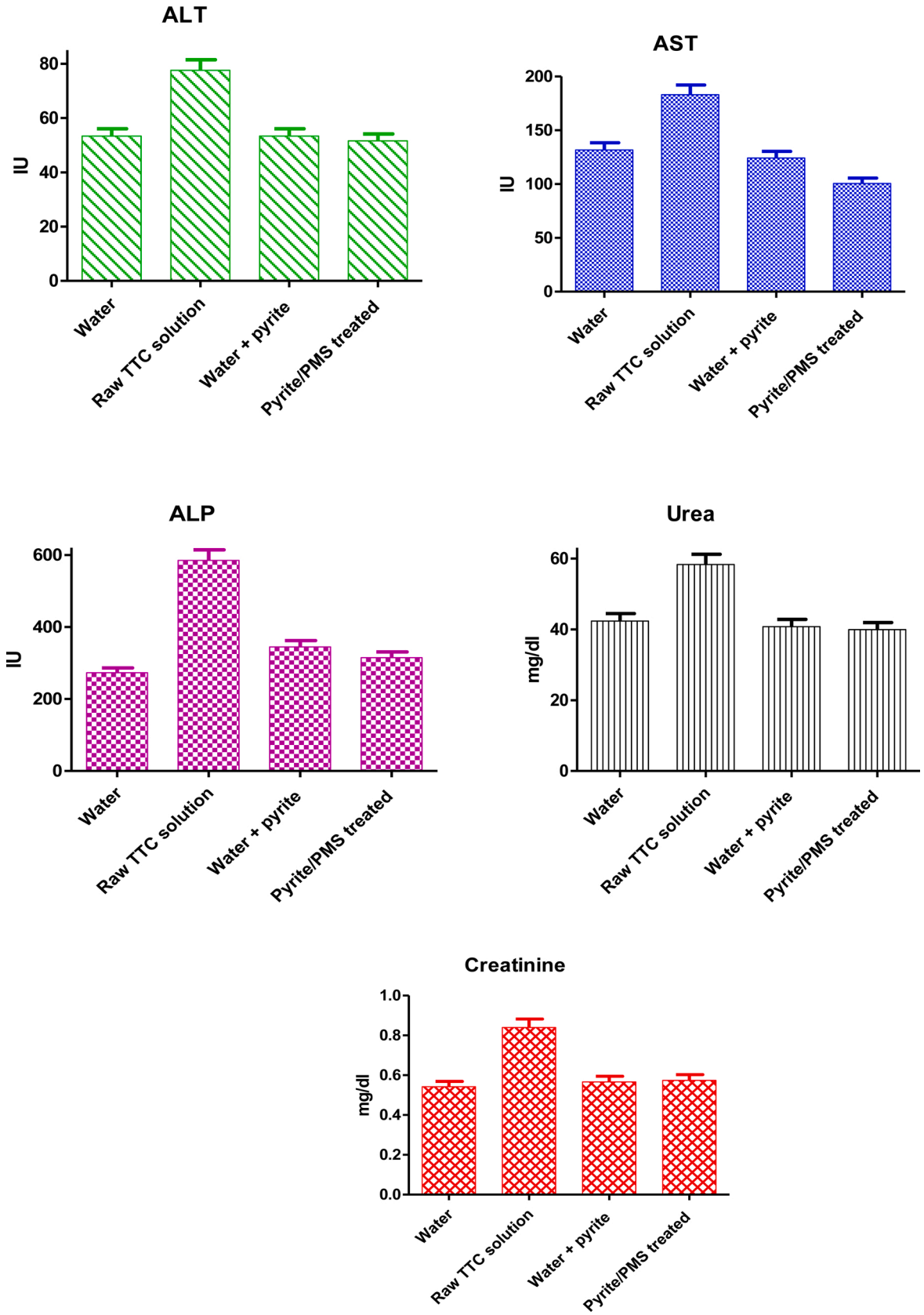

Fig. 17. Effect of TTC solution treatment on liver enzyme (ALT, AST and ALP) and kidney function tests (urea and creatinine).

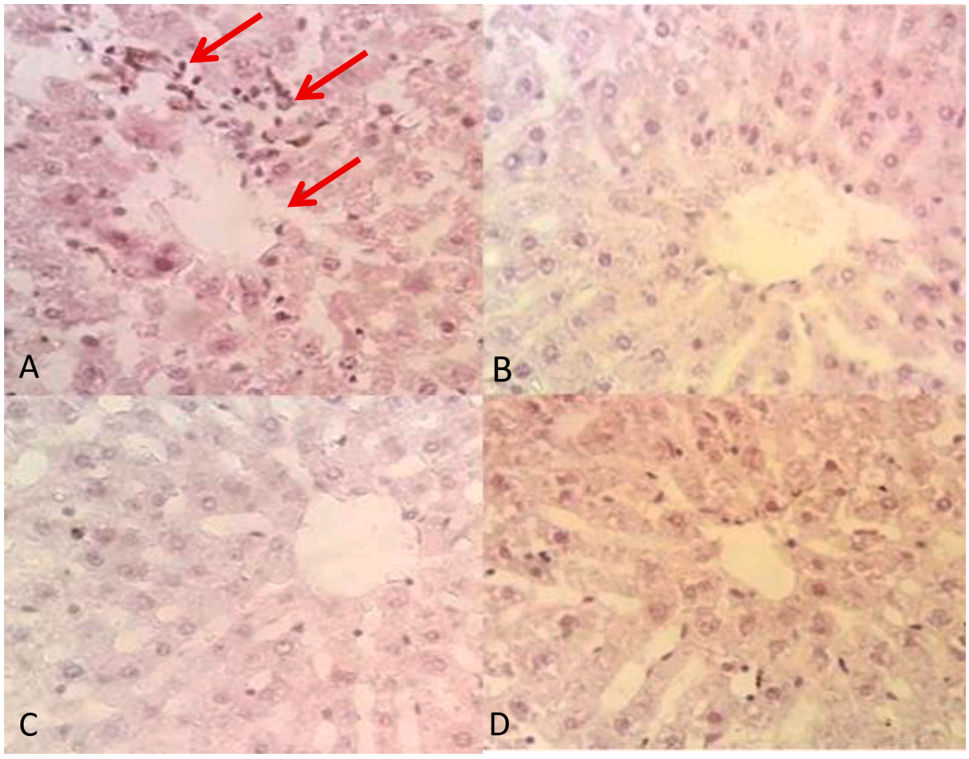

Fig. 18. Effect of TTC solution treatment on liver tissue (HE staining X400). A: raw TTC solution, B: pyrite/PMS TTC treated solution, C: water solution containing pyrite and D: pure water solution.

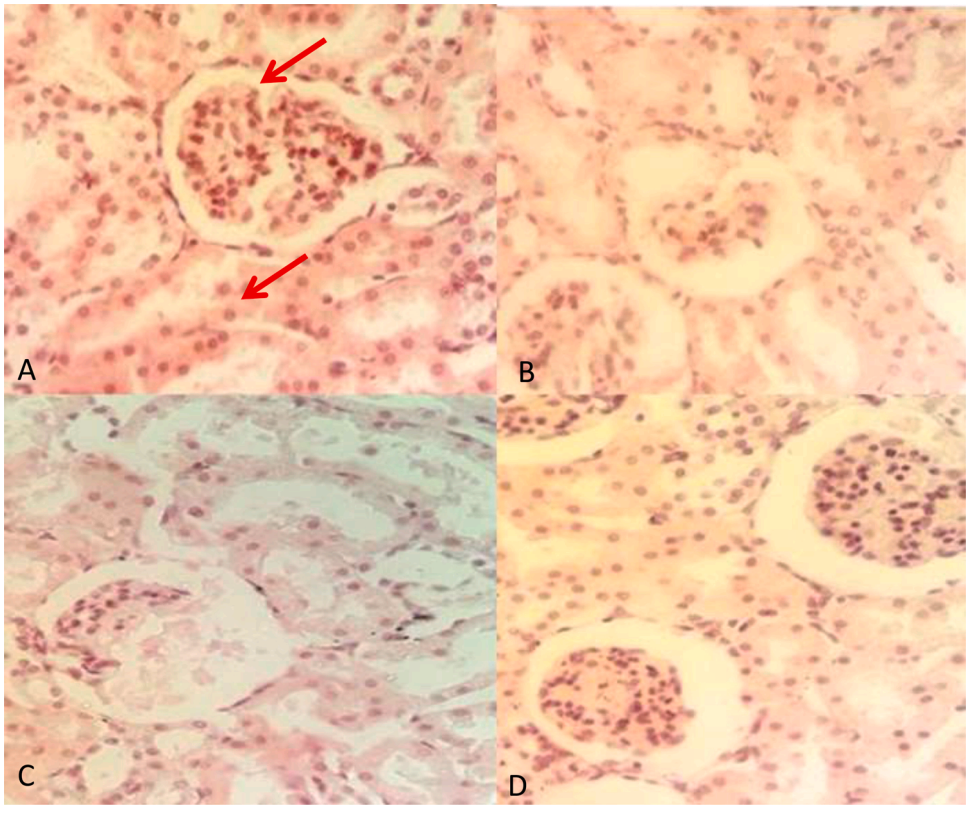

Fig. 19. Effect of TTC solution treatment on kidney tissue (HE staining X400). A: raw TTC solution B: pyrite/PMS TTC treated solution, C: water solution containing pyrite and D: pure water solution.

Approval is granted on the conditions outlined below.

- Prior approval from the Ethics Committee is required before implementing any changes in the consent documents or any changes in the protocol unless those changes are required urgently for the subjects.
- You must complete and return the final report form when your research is completed.

Declaration of Competing Interest

The authors declare that they have no known competing financial interests or personal relationships that could have appeared to influence the work reported in this paper.

Acknowledgements

The authors gratefully acknowledge the financial (Grant No, 97101) and technical support provided by Shahroud University of Medical Sciences. S.R. acknowledges the Chevreul Institute (FR 2638), the Ministère de l'Enseignement Supérieur et de la Recherche, the Région Hauts-de-France, the FEDER for supporting and funding partially this work.

Appendix A. Supplementary data

Supplementary material related to this article can be found, in the online version, at doi:https://doi.org/10.1016/j.jwpe.2020.101808.

References

[1] F. Fanaei, G. Moussavi, V. Srivastava, M. Sillanpää, The enhanced catalytic potential of sulfur-doped MgO (S-MgO) nanoparticles in activation of peroxysulfates for advanced oxidation of acetaminophen, Chem. Eng. J. 371 (2019) 404–413, https://doi.org/10.1016/j.cej.2019.04.007.

[2] F. Rashidashmagh, Y. Doekhi-Bennani, M. Tizghadam-Ghazani, J.P. van der Hoek, A. Mashayekh-Salehi, B.S.G.J. Heijman, K. Yaghmaeian, Synthesis and characterization of SnO2crystalline nanoparticles: a new approach for enhancing the catalytic ozonation of acetaminophen, J. Hazard. Mater. 404 (2021), https://doi.org/10.1016/j.jhazmat.2020.124154.

[3] Z. Yousefi, A. Mashayekh-Salehi, R.A. Mohammadpour Tahmtan, Biosorption of chromium in aqueous solutions using Bivalve Mollusk Shells through central composite design (CCD) model, Desalin. Water Treat. 57 (2016), https://doi.org/10.1080/19443994.2015.1106342.

[4] A. Mashayekh-Salehi, G. Moussavi, Removal of acetaminophen from the contaminated water using adsorption onto carbon activated with NH4Cl, Desalin. Water Treat. 57 (2016), https://doi.org/10.1080/19443994.2015.1051588.

[5] U.A. Qureshi, B.H. Hameed, M.J. Ahmed, Adsorption of endocrine disrupting compounds and other emerging contaminants using lignocellulosic biomass-derived porous carbons: a review, J. Water Process Eng. 38 (2020), https://doi.org/10.1016/j.jwpe.2020.101380.

[6] G. Moussavi, A. Mashayekh-Salehi, K. Yaghmaeian, A. Mohseni-Bandpei, The catalytic destruction of antibiotic tetracycline by sulfur-doped manganese oxide (S–MgO) nanoparticles, J. Environ. Manage. 210 (2018) 131–138, https://doi.org/10.1016/j.jenvman.2018.01.004.

[7] A. Mashayekh-Salehi, G. Moussavi, K. Yaghmaeian, Preparation, characterization and catalytic activity of a novel mesoporous nanocrystalline MgO nanoparticle for ozonation of acetaminophen as an emerging water contaminant, Chem. Eng. J. 310 (2017), https://doi.org/10.1016/j.cej.2016.10.096.

[8] W. Song, J. Li, Z. Wang, X. Zhang, A mini review of activated methods to persulfate-based advanced oxidation process, Water Sci. Technol. 79 (2019) 573–579, https://doi.org/10.2166/wcc.2018.168.

[9] G.D. Fang, D.D. Dionysiou, S.R. Al-Abed, D.M. Zhou, Superoxide radical driving the activation of persulfate by magnetite nanoparticles: implications for the degradation of PCBs, Appl. Catal. B Environ. 129 (2013) 325–332, https://doi.org/10.1016/j.apcatb.2012.09.042.

[10] K. Yaghmaeian, G. Moussavi, A. Mashayekh-Salehi, A. Mohseni-Bandpei, M. Satari, Oxidation of acetaminophen in the ozonation process catalyzed with modified MgO nanoparticles: effect of operational variables and cytotoxicity assessment, Process Saf. Environ. Prot. 109 (2017) 520–528, https://doi.org/10.1016/j.psep.2017.04.020.

[11] L. Hou, H. Zhang, X. Xue, Ultrasound enhanced heterogeneous activation of peroxydisulfate by magnetite catalyst for the degradation of tetracycline in water, Sep. Purif. Technol. 84 (2012) 147–152.

[12] D. Xia, Y. Li, G. Huang, R. Yin, T. An, G. Li, H. Zhao, A. Lu, P.K. Wong, Activation of persulfates by natural magnetic pyrrhotite for water disinfection: Efficiency, mechanisms, and stability, Water Res. 112 (2017) 236–247, https://doi.org/10.1016/j.watres.2017.01.052.

[13] S. Yang, P. Wang, X. Yang, L. Shan, W. Zhang, X. Shao, R. Niu, Degradation efficiencies of azo dye acid orange 7 by the interaction of heat, UV and anions with common oxidants: persulfate, peroxymonosulfate and hydrogen peroxide, J. Hazard. Mater. 179 (2010) 552–558, https://doi.org/10.1016/j.jhazmat.2010.03.039.

[14] A. Ghauch, A.M. Tuqan, N. Kibbi, Ibuprofen removal by heated persulfate in aqueous solution: a kinetics study, Chem. Eng. J. 197 (2012) 483–492, https://doi.org/10.1016/j.cej.2012.05.051.

[15] Y. Zhang, Q. Zhang, J. Hong, Sulfate radical degradation of acetaminophen by novel iron–copper bimetallic oxidation catalyzed by persulfate: mechanism and degradation pathways, Appl. Surf. Sci. 422 (2017) 443–453, https://doi.org/10.1016/j.apsusc.2017.05.224.

[16] F. Velichkova, C. Julcour-Lebigue, B. Koumanova, H. Delmas, Heterogeneous Fenton oxidation of paracetamol using iron oxide (nano) particles, J. Environ. Chem. Eng. 1 (2013) 1214–1222.

[17] A. Ghauch, G. Ayoub, S. Naim, Degradation of sulfamethoxazole by persulfate assisted micrometric Fe0 in aqueous solution, Chem. Eng. J. 228 (2013) 1168–1181, https://doi.org/10.1016/j.cej.2013.05.045.

[18] G. Ayoub, A. Ghauch, Assessment of bimetallic and trimetallic iron-based systems for persulfate activation: application to sulfamethoxazole degradation, Chem. Eng. J. 256 (2014) 280–292, https://doi.org/10.1016/j.cej.2014.07.002.

[19] Y. Chen, J. Yan, D. Ouyang, L. Qian, L. Han, M. Chen, Heterogeneously catalyzed persulfate by CuMgFe layered double oxide for the degradation of phenol, Appl. Catal. A Gen. 538 (2017) 19–26, https://doi.org/10.1016/j.apcata.2017.03.020.

[20] C. Tan, N. Gao, D. Fu, J. Deng, L. Deng, Efficient degradation of paracetamol with nanoscaled magnetic CoFe2O4 and MnFe2O4 as a heterogeneous catalyst of peroxymonosulfate, Sep. Purif. Technol. 175 (2017) 47–57, https://doi.org/10.1016/j.seppur.2016.11.016.

[21] Q. Wang, Y. Shao, N. Gao, W. Chu, J. Chen, X. Lu, Y. Zhu, N. An, Activation of peroxymonosulfate by Al_2O_3-based $CoFe_2O_4$ for the degradation of sulfachloropyridazine sodium: kinetics and mechanism, Sep. Purif. Technol. 189 (2017) 176–185, https://doi.org/10.1016/j.seppur.2017.07.046.

[22] Z.H. Diao, J.J. Liu, Y.X. Hu, L.J. Kong, D. Jiang, X.R. Xu, Comparative study of Rhodamine B degradation by the systems pyrite/H2O2 and pyrite/persulfate: reactivity, stability, products and mechanism, Sep. Purif. Technol. 184 (2017) 374–383, https://doi.org/10.1016/j.seppur.2017.05.016.

[23] S. Chen, P. Xiong, W. Zhan, L. Xiong, Degradation of ethylthionocarbamate by pyrite-activated persulfate, Miner. Eng. 122 (2018) 38–43.

[24] C. Liang, Y.Y. Guo, Y.C. Chien, Y.J. Wu, Oxidative degradation of MTBE by pyrite-activated persulfate: proposed reaction pathways, Ind. Eng. Chem. Res. 49 (2010) 8858–8864, https://doi.org/10.1021/ie100740d.

[25] S. Chen, P. Xiong, W. Zhan, L. Xiong, Degradation of ethylthionocarbamate by pyrite-activated persulfate, Miner. Eng. 122 (2018) 38–43, https://doi.org/10.1016/j.mineng.2018.03.022.

[26] T.S. Jamil, H. Roland, H. Michael, R. Jens-Uwe, Homogeneous photocatalytic processes for degradation of some endocrine disturbing chemicals under UV irradiation, J. Water Process Eng. 18 (2017) 159–168, https://doi.org/10.1016/j.jwpe.2017.04.005.

[27] C. Cai, H. Zhang, X. Zhong, L. Hou, Electrochemical enhanced heterogeneous activation of peroxydisulfate by Fe-Co/SBA-15 catalyst for the degradation of Orange II in water, Water Res. 66 (2014) 473–485, https://doi.org/10.1016/j.watres.2014.08.039.

[28] Y. Zhang, K. Zhang, C. Dai, X. Zhou, H. Si, An enhanced Fenton reaction catalyzed by natural heterogeneous pyrite for nitrobenzene degradation in an aqueous solution, Chem. Eng. J. 224 (2014) 438–445, https://doi.org/10.1016/j.cej.2014.01.088.

[29] K.Y.A. Lin, Z.Y. Zhang, T. Wi-Afedzi, Sulfur-doped carbon nitride as a non-metal heterogeneous catalyst for sulfate radical-based advanced oxidation processes in the absence of light irradiation, J. Water Process Eng. 24 (2018) 83–89, https://doi.org/10.1016/j.jwpe.2018.02.018.

[30] C.C. Lin, M.S. Wu, Performance of a large reactor in degrading sulfamethazine in water using UV and persulfate, J. Water Process Eng. 31 (2019), https://doi.org/10.1016/j.jwpe.2019.100874.

[31] M.A. Shaida, A.K. Sen, R.K. Dutta, Alternate use of sulphur rich coals as solar photo-Fenton agent for degradation of toxic azo dyes, J. Clean. Prod. 195 (2018) 1003–1014, https://doi.org/10.1016/j.jclepro.2018.05.286.

[32] S. Fathinia, M. Fathinia, A.A. Rahmani, A. Khataee, Preparation of natural pyrite nanoparticles by high energy planetary ball milling as a nanocatalyst for heterogeneous Fenton process, Appl. Surf. Sci. 327 (2015) 190–200, https://doi.org/10.1016/j.apsusc.2014.11.157.

[33] O. Oral, C. Kantar, Diclofenac removal by pyrite-Fenton process: performance in batch and fixed-bed continuous flow systems, Sci. Total Environ. 664 (2019) 817–823, https://doi.org/10.1016/j.scitotenv.2019.02.084.

[34] C. Kantar, O. Oral, N.A. Oz, Ligand enhanced pharmaceutical wastewater treatment with Fenton process using pyrite as the catalyst: column experiments, Chemosphere 237 (2019), https://doi.org/10.1016/j.chemosphere.2019.124440.

[35] N. Barhoumi, N. Oturan, H. Olvera-Vargas, E. Brillas, A. Gadri, S. Ammar, M. A. Oturan, Pyrite as a sustainable catalyst in electro-Fenton process for improving oxidation of sulfamethazine. Kinetics, mechanism and toxicity assessment, Water Res. 94 (2016) 52–61.

[36] Y. Zhang, H.P. Tran, X. Du, I. Hussain, S. Huang, S. Zhou, W. Wen, Efficient pyrite activating persulfate process for degradation of p-chloroaniline in aqueous systems: a mechanistic study, Chem. Eng. J. 308 (2017) 1112–1119, https://doi.org/10.1016/j.cej.2016.09.104.

[37] H.T. Pham, M. Kitsuneduka, J. Hara, K. Suto, C. Inoue, Trichloroethylene transformation by natural mineral pyrite: the deciding role of oxygen, Environ. Sci. Technol. 42 (2008) 7470–7475.
[38] A. Khataee, P. Gholami, M. Sheydaei, S. Khorram, S.W. Joo, Preparation of nanostructured pyrite with N 2 glow discharge plasma and the study of its catalytic performance in the heterogeneous Fenton process, New J. Chem. 40 (2016) 5221–5230.
[39] Q.Q. Zhang, G.G. Ying, C.G. Pan, Y.S. Liu, J.L. Zhao, Comprehensive evaluation of antibiotics emission and fate in the river basins of China: source analysis, multimedia modeling, and linkage to bacterial resistance, Environ. Sci. Technol. 49 (2015) 6772–6782, https://doi.org/10.1021/acs.est.5b00729.
[40] Z.Y. Lu, Y.L. Ma, J.T. Zhang, N.S. Fan, B.C. Huang, R.C. Jin, A critical review of antibiotic removal strategies: performance and mechanisms, J. Water Process Eng. 38 (2020), https://doi.org/10.1016/j.jwpe.2020.101681.
[41] A.J. Watkinson, E.J. Murby, S.D. Costanzo, Removal of antibiotics in conventional and advanced wastewater treatment: implications for environmental discharge and wastewater recycling, Water Res. 41 (2007) 4164–4176, https://doi.org/10.1016/j.watres.2007.04.005.
[42] X.S. Miao, F. Bishay, M. Chen, C.D. Metcalfe, Occurrence of antimicrobials in the final effluents of wastewater treatment plants in Canada, Environ. Sci. Technol. 38 (2004) 3533–3541, https://doi.org/10.1021/es030653q.
[43] S. Jiao, S. Zheng, D. Yin, L. Wang, L. Chen, Aqueous photolysis of tetracycline and toxicity of photolytic products to luminescent bacteria, Chemosphere 73 (2008) 377–382.
[44] S. Al Aani, T.N. Mustafa, N. Hilal, Ultrafiltration membranes for wastewater and water process engineering: a comprehensive statistical review over the past decade, J. Water Process Eng. 35 (2020), https://doi.org/10.1016/j.jwpe.2020.101241.
[45] Z. Cetecioglu, B. Ince, M. Gros, S. Rodriguez-Mozaz, D. Barceló, D. Orhon, O. Ince, Chronic impact of tetracycline on the biodegradation of an organic substrate mixture under anaerobic conditions, Water Res. 47 (2013) 2959–2969, https://doi.org/10.1016/j.watres.2013.02.053.
[46] M.H. Huang, W. Zhang, C. Liu, H.Y. Hu, Fate of trace tetracycline with resistant bacteria and resistance genes in an improved AAO wastewater treatment plant, Process Saf. Environ. Prot. 93 (2015) 68–74, https://doi.org/10.1016/j.psep.2014.04.004.
[47] J.S. Davis, R.H. Kaufman, Tetracycline toxicity. A clinicopathologic study with special reference to liver damage and its relationship to pregnancy, Am. J. Obstet. Gynecol. 93 (1966) 523–529, https://doi.org/10.1016/0002-9378(66)90144-X.
[49] Y. Zhang, J. Geng, H. Ma, H. Ren, K. Xu, L. Ding, Characterization of microbial community and antibiotic resistance genes in activated sludge under tetracycline and sulfamethoxazole selection pressure, Sci. Total Environ. 571 (2016) 479–486, https://doi.org/10.1016/j.scitotenv.2016.07.014.
[50] C. Zhou, Z. Zeng, G. Zeng, D. Huang, R. Xiao, M. Cheng, C. Zhang, W. Xiong, C. Lai, Y. Yang, W. Wang, H. Yi, B. Li, Visible-light-driven photocatalytic degradation of sulfamethazine by surface engineering of carbon nitride: properties, degradation pathway and mechanisms, J. Hazard. Mater. 380 (2019) 120815, https://doi.org/10.1016/j.jhazmat.2019.120815.
[51] C. Zhou, D. Huang, P. Xu, G. Zeng, J. Huang, T. Shi, C. Lai, C. Zhang, M. Cheng, Y. Lu, A. Duan, W. Xiong, M. Zhou, Efficient visible light driven degradation of sulfamethazine and tetracycline by salicylic acid modified polymeric carbon nitride via charge transfer, Chem. Eng. J. 370 (2019) 1077–1086, https://doi.org/10.1016/j.cej.2019.03.279.
[52] C. Zhou, G. Zeng, D. Huang, Y. Luo, M. Cheng, Y. Liu, W. Xiong, Y. Yang, B. Song, W. Wang, B. Shao, Z. Li, Distorted polymeric carbon nitride via carriers transfer bridges with superior photocatalytic activity for organic pollutants oxidation and hydrogen production under visible light, J. Hazard. Mater. 386 (2020), https://doi.org/10.1016/j.jhazmat.2019.121947.
[53] T. Olmez-Hanci, I. Arslan-Alaton, D. Dursun, Investigation of the toxicity of common oxidants used in advanced oxidation processes and their quenching agents, J. Hazard. Mater. 278 (2014) 330–335, https://doi.org/10.1016/j.jhazmat.2014.06.021.
[54] Standard methods for the examination of water and wastewater, Choice Rev. Online (2012), https://doi.org/10.5860/choice.49-6910.
[55] Y. Zhang, K. Zhang, C. Dai, X. Zhou, Performance and mechanism of pyrite for nitrobenzene removal in aqueous solution, Chem. Eng. Sci. 111 (2014) 135–141.
[56] S. Bae, D. Kim, W. Lee, Degradation of diclofenac by pyrite catalyzed Fenton oxidation, Appl. Catal. B Environ. 134 (2013) 93–102.
[57] L. Labiadh, M.A. Oturan, M. Panizza, N. Ben Hamadi, S. Ammar, Complete removal of AHPS synthetic dye from water using new electro-fenton oxidation catalyzed by natural pyrite as heterogeneous catalyst, J. Hazard. Mater. 297 (2015) 34–41, https://doi.org/10.1016/j.jhazmat.2015.04.062.
[58] Z.-H. Diao, J.-J. Liu, Y.-X. Hu, L.-J. Kong, D. Jiang, X.-R. Xu, Comparative study of Rhodamine B degradation by the systems pyrite/H_2O_2 and pyrite/persulfate: reactivity, stability, products and mechanism, Sep. Purif. Technol. 184 (2017) 374–383.
[59] A. Khataee, P. Gholami, B. Vahid, Heterogeneous sono-Fenton-like process using nanostructured pyrite prepared by Ar glow discharge plasma for treatment of a textile dye, Ultrason. Sonochem. 29 (2016) 213–225.
[60] X. Yang, X. Zhang, Z. Wang, S. Li, J. Zhao, G. Liang, X. Xie, Mechanistic insights into removal of norfloxacin from water using different natural iron ore – biochar composites: more rich free radicals derived from natural pyrite-biochar composites than hematite-biochar composites, Appl. Catal. B Environ. 255 (2019), https://doi.org/10.1016/j.apcatb.2019.117752.
[61] A. Khataee, S. Fathinia, M. Fathinia, Production of pyrite nanoparticles using high energy planetary ball milling for sonocatalytic degradation of sulfasalazine, Ultrason. Sonochem. 34 (2017) 904–915.
[62] C. Kantar, O. Oral, O. Urken, N.A. Oz, Role of complexing agents on oxidative degradation of chlorophenolic compounds by pyrite-Fenton process: batch and column experiments, J. Hazard. Mater. 373 (2019) 160–167, https://doi.org/10.1016/j.jhazmat.2019.03.065.
[63] A. Rastogi, S.R. Al-Abed, D.D. Dionysiou, Sulfate radical-based ferrous-peroxymonosulfate oxidative system for PCBs degradation in aqueous and sediment systems, Appl. Catal. B Environ. 85 (2009) 171–179, https://doi.org/10.1016/j.apcatb.2008.07.010.
[64] T. Olmez-Hanci, I. Arslan-Alaton, Comparison of sulfate and hydroxyl radical based advanced oxidation of phenol, Chem. Eng. J. 224 (2013) 10–16, https://doi.org/10.1016/j.cej.2012.11.007.
[65] G. Moussavi, M. Pourakbar, E. Aghayani, M. Mahdavianpour, Investigating the aerated VUV/PS process simultaneously generating hydroxyl and sulfate radicals for the oxidation of cyanide in aqueous solution and industrial wastewater, Chem. Eng. J. 350 (2018) 673–680.
[66] Y. Yuan, H. Tao, J. Fan, L. Ma, Degradation of p-chloroaniline by persulfate activated with ferrous sulfide ore particles, Chem. Eng. J. 268 (2015) 38–46, https://doi.org/10.1016/j.cej.2014.12.092.
[67] H. Chen, Z. Zhang, M. Feng, W. Liu, W. Wang, Q. Yang, Y. Hu, Degradation of 2,4-dichlorophenoxyacetic acid in water by persulfate activated with FeS (mackinawite), Chem. Eng. J. 313 (2017) 498–507, https://doi.org/10.1016/j.cej.2016.12.075.
[68] G. Moussavi, H. Momeninejad, S. Shekoohiyan, P. Baratpour, Oxidation of acetaminophen in the contaminated water using UVC/S2O82− process in a cylindrical photoreactor: efficiency and kinetics of degradation and mineralization, Sep. Purif. Technol. 181 (2017) 132–138, https://doi.org/10.1016/j.seppur.2017.03.022.
[69] L. Hou, L. Wang, S. Royer, H. Zhang, Ultrasound-assisted heterogeneous Fenton-like degradation of tetracycline over a magnetite catalyst, J. Hazard. Mater. 302 (2016) 458–467.
[70] X. Wang, Y. Wang, N. Chen, Y. Shi, L. Zhang, Pyrite enables persulfate activation for efficient atrazine degradation, Chemosphere 224 (2020), https://doi.org/10.1016/j.chemosphere.2019.125568.
[71] S.Y. Oh, S.G. Kang, D.W. Kim, P.C. Chiu, Degradation of 2,4-dinitrotoluene by persulfate activated with iron sulfides, Chem. Eng. J. 172 (2011) 641–646, https://doi.org/10.1016/j.cej.2011.06.023.
[72] S. Peng, Y. Feng, Y. Liu, D. Wu, Applicability study on the degradation of acetaminophen via an H2O2/PDS-based advanced oxidation process using pyrite, Chemosphere 212 (2018) 438–446.
[73] W. Lian, X. Yi, K. Huang, T. Tang, R. Wang, X. Tao, Z. Zheng, Z. Dang, H. Yin, G. Lu, Degradation of tris (2-chloroethyl) phosphate (TCEP) in aqueous solution by using pyrite activating persulfate to produce radicals, Ecotoxicol. Environ. Saf. 174 (2019) 667–674.
[74] X. Zhang, Y. Qin, W. Zhang, Y. Zhang, G.E. Yuan, Oxidative degradation of Orange G in aqueous solution by persulfate activated with pyrite, Water Sci. Technol. 82 (2020) 185–193, https://doi.org/10.2166/wst.2020.352.
[75] X.R. Xu, X.Z. Li, Degradation of azo dye Orange G in aqueous solutions by persulfate with ferrous ion, Sep. Purif. Technol. 72 (2010) 105–111, https://doi.org/10.1016/j.seppur.2010.01.012.
[76] R.L. López, O. Coreño, J.L. Nava, Abatement of hydrated silica and simultaneous removal of coexisting ions from deep well water by electrocoagulation using an up-flow reactor, J. Water Process Eng. 32 (2019), https://doi.org/10.1016/j.jwpe.2019.100923.
[77] X. Wu, X. Gu, S. Lu, Z. Qiu, Q. Sui, X. Zang, Z. Miao, M. Xu, Strong enhancement of trichloroethylene degradation in ferrous ion activated persulfate system by promoting ferric and ferrous ion cycles with hydroxylamine, Sep. Purif. Technol. 147 (2015) 186–193, https://doi.org/10.1016/j.seppur.2015.04.031.
[78] Y.F. Rao, L. Qu, H. Yang, W. Chu, Degradation of carbamazepine by Fe(II)-activated persulfate process, J. Hazard. Mater. 268 (2014) 23–32, https://doi.org/10.1016/j.jhazmat.2014.01.010.
[79] X. Wei, N. Gao, C. Li, Y. Deng, S. Zhou, L. Li, Zero-valent iron (ZVI) activation of persulfate (PS) for oxidation of bentazon in water, Chem. Eng. J. 285 (2016) 660–670, https://doi.org/10.1016/j.cej.2015.08.120.
[80] Y. Liu, X. He, X. Duan, Y. Fu, D.D. Dionysiou, Photochemical degradation of oxytetracycline: influence of pH and role of carbonate radical, Chem. Eng. J. 276 (2015) 1113–1121, https://doi.org/10.1016/j.cej.2015.04.048.
[81] X. Ao, W. Sun, S. Li, C. Yang, C. Li, Z. Lu, Degradation of tetracycline by medium pressure UV-activated peroxymonosulfate process: influencing factors, degradation pathways, and toxicity evaluation, Chem. Eng. J. 361 (2019) 1053–1062, https://doi.org/10.1016/j.cej.2018.12.133.
[82] L. Wojnárovits, T. Tóth, E. Takács, Rate constants of carbonate radical anion reactions with molecules of environmental interest in aqueous solution: a review, Sci. Total Environ. 717 (2020) 137219, https://doi.org/10.1016/j.scitotenv.2020.137219.